OPEN ACCESS Freely available online

PLoS GENETICS

H3 Lysine 4 Is Acetylated at Active Gene Promoters and Is Regulated by H3 Lysine 4 Methylation

Benoit Guillemette[1,2], Paul Drogaris[2], Hsiu-Hsu Sophia Lin[1], Harry Armstrong[2], Kyoko Hiragami-Hamada[3], Axel Imhof[4], Éric Bonneil[2], Pierre Thibault[2,5], Alain Verreault[2,6], Richard J. Festenstein[1,7]*

1 Department of Medicine, Imperial College London, Hammersmith Hospital Campus, London, United Kingdom, **2** Institute for Research in Immunology and Cancer, Université de Montréal, Montréal, Canada, **3** Laboratory for Chromatin Dynamics, Riken Kobe Institute, Centre for Developmental Biology, Kobe, Hyogo, Japan, **4** Adolf-Butenandt Institute, Ludwig-Maximilians-University Munich (LMU), Center of Integrated Protein Science (CIPS), Munich, Germany, **5** Département de Chimie, Université de Montréal, Montreal, Canada, **6** Département de Pathologie et Biologie Cellulaire, Université de Montréal, Montreal, Canada, **7** Medical Research Council Clinical Sciences Centre, London, United Kingdom

Abstract

Methylation of histone H3 lysine 4 (H3K4me) is an evolutionarily conserved modification whose role in the regulation of gene expression has been extensively studied. In contrast, the function of H3K4 acetylation (H3K4ac) has received little attention because of a lack of tools to separate its function from that of H3K4me. Here we show that, in addition to being methylated, H3K4 is also acetylated in budding yeast. Genetic studies reveal that the histone acetyltransferases (HATs) Gcn5 and Rtt109 contribute to H3K4 acetylation *in vivo*. Whilst removal of H3K4ac from euchromatin mainly requires the histone deacetylase (HDAC) Hst1, Sir2 is needed for H3K4 deacetylation in heterochomatin. Using genome-wide chromatin immunoprecipitation (ChIP), we show that H3K4ac is enriched at promoters of actively transcribed genes and located just upstream of H3K4 tri-methylation (H3K4me3), a pattern that has been conserved in human cells. We find that the Set1-containing complex (COMPASS), which promotes H3K4me2 and -me3, also serves to limit the abundance of H3K4ac at gene promoters. In addition, we identify a group of genes that have high levels of H3K4ac in their promoters and are inadequately expressed in *H3-K4R*, but not in *set1*Δ mutant strains, suggesting that H3K4ac plays a positive role in transcription. Our results reveal a novel regulatory feature of promoter-proximal chromatin, involving mutually exclusive histone modifications of the same histone residue (H3K4ac and H3K4me).

Citation: Guillemette B, Drogaris P, Lin H-HS, Armstrong H, Hiragami-Hamada K, et al. (2011) H3 Lysine 4 Is Acetylated at Active Gene Promoters and Is Regulated by H3 Lysine 4 Methylation. PLoS Genet 7(3): e1001354. doi:10.1371/journal.pgen.1001354

Editor: Hiten D. Madhani, University of California San Francisco, United States of America

Received April 7, 2010; **Accepted** February 25, 2011; **Published** March 31, 2011

Funding: BG was the recipient of a Canada/USA Incoming Fellowship from The Royal Society (UK; http://royalsociety.org/). Part of this research was funded by grants from the Medical Research Council Research Council (G0301153 and U.1200.05.001.00001; UK; www.mrc.ac.uk) to RJF, the Canadian Institutes for Health Research (89928; www.cihr-irsc.gc.ca) to AV, and the Natural Sciences and Engineering Council of Canada (311598-08; www.nserc-crsng.gc.ca) to PT. IRICs infrastructure is supported by funds from the Canadian Centre of Excellence in Commercialisation and Research (www.rce-nce.gc.ca), the Canadian Foundation for Innovation (www.innovation.ca), and the Fonds de Recherche en Sante du Quebec (www.frsq.gouv.qc.ca). The funders had no role in study design, data collection and analysis, decision to publish, or preparation of the manuscript.

Competing Interests: The authors have declared that no competing interests exist.

* E-mail: r.festenstein@imperial.ac.uk

Introduction

Histones are covalently modified on many lysine residues. The outcome of these modifications is either to modify chromatin structure directly or provide docking sites for the binding of non-histone proteins [1]. The same chemical modification (*e.g.* methylation) on different residues can lead to distinct outcomes. Moreover, some histone modifications function in a combinatorial fashion to generate different functional outcomes [2-4]. This led to the notion that histone modifications may represent an epigenetic code that influences gene expression and serves as a "memory" of cell identity during development of cell lineages [5-6]. The recent development of high resolution mass spectrometry has enabled the identification of a great number of new histone modifications [7-9]. Elucidation of the functions of these new modifications is greatly facilitated in model organisms where, in contrast to vertebrate cells, histone gene mutations that abolish specific modifications can be readily introduced.

Histone H3 lysine 4 is a highly studied residue whose modification is important for many biological processes in a wide range of species [10-11]. The genomic localisation of H3K4 methylation (H3K4me) has been conserved through evolution. It is highly regulated and generally associated with transcriptionally active genes [12-18]. H3K4 tri-methylation (H3K4me3) is a hallmark of transcriptional start sites and is generally followed by H3K4me2 and H3K4me1 along gene coding regions [19-22]. The multiple functions of H3K4 are mediated by a number of chromatin-associated proteins that selectively bind to some of the four methylation states of H3K4: unmethylated, mono-, di- or trimethylated [23-37]. In yeast, H3K4 is methylated by Set1, a SET domain containing protein and a homolog of Trithorax. Set1 is part of a complex termed COMPASS (complex of proteins asociated with Set1) [38-42]. The regulation of the different forms of H3K4me is complex and requires not only the components of COMPASS, but also a *trans*-histone pathway which involves mono-ubiquitylation of H2B lysine 123 [43-44].

A close link exists between H3K4me2 and -me3 and acetylation of the H3 tail. H3K4me3 is often found together with acetylation of other residues (*i.e.* K9, K14, K18, K23 and K27) on the same H3 molecules [45-49]. In a subset of yeast genes, H3K4me3

Author Summary

In the nucleus of mammals and yeast, DNA is packaged by forming complexes with histone proteins in a structure called the nucleosome, the basic building block of chromatin. The tails of the histones protrude from the nucleosome and can be marked on many amino acid residues by chemical modifications such as methylation and acetylation. A highly studied modification, which is robustly associated with active gene promoters, is histone H3 lysine 4 methylation. We describe here a novel modification, histone H3 lysine 4 acetylation (H3K4ac), which can occur on the same lysine of the histone H3 tail (but not at the same time as methylation). We have identified the enzymes responsible for depositing and removing this mark and mapped its distribution throughout the yeast genome. We found that H3K4ac is present on active genes and is important for the full expression of a subset of them. Strikingly, H3K4 methylation was found in the same promoters as H3K4ac and contributes to regulate the abundance and localisation of H3K4ac. This example of cross-talk between two different modifications of the same residue has fundamental implications for understanding how genes are activated and how their packaging in the nucleus controls this process.

directly binds to the PHD finger domain of Yng1, a subunit of the NuA3 histone acetyltransferase (HAT) complex that modifies H3K14, which couples the acetylation and methylation of H3 on different residues [33]. In contrast, through the recruitment of the SET3 complex, H3K4me2 in coding regions promotes deacetylation of H3 in the wake of RNA polymerase II (RNApol II) [50]. These results suggest that there is a highly dynamic and coordinated interplay between histone H3K4 methylation and the enzymes that control H3 acetylation during transcription.

Despite extensive studies of histone H3K4 methylation, the functional implications of other modifications that occur on the same residue have not been investigated. Here, we identified H3K4 acetylation (H3K4ac) in *S. cerevisiae* using mass spectrometry and a highly specific antibody that we developed. We found that *GCN5* and, to a lesser extent, *RTT109* are needed for both H3K4ac and H3K9ac *in vivo*. H3K4 deacetylation in euchromatin is mainly dependent upon *HST1*, and partly on *SIR2*. In contrast, removal of H3K4ac from heterochromatin requires *SIR2* only. Genome-wide ChIP experiments revealed that H3K4ac is generally found upstream of H3K4me3 in active gene promoters, a pattern which has been conserved at many human $CD4^+$ T-cell promoters [51]. We further demonstrate that H3K4me2 and –me3 mediated by the COMPASS complex limits global levels of H3K4ac at promoters and prevents it from spreading into the 5′-ends of coding regions. Using a genetic approach to separate the functions of H3K4ac and H3K4me, we identified a subset of *S. cerevisiae* genes whose expression depends upon H3K4ac, but not H3K4me. Altogether, our results strongly support a positive role for H3K4ac in gene transcription and identify a novel interplay between two modifications of the same histone residue.

Results

Histone H3 lysine 4 is acetylated in *Saccharomyces cerevisiae*

One of the most studied and conserved histone modifications is H3K4 methylation (H3K4me), which is tightly linked to transcription in many species [10]. Because of this, and the fact that methylation and acetylation of the same lysine residue are mutually exclusive, we investigated whether H3K4ac was present in *S. cerevisiae*, a powerful model organism for genetic analysis. For this purpose, we raised an antibody against H3K4ac and confirmed its specificity with peptide binding assays and immunoblotting competition assays (Figure 1A, 1B). Previous studies have detected the presence of H3K4ac in human cells and an antibody was made commercially available, however the specificity of this antibody was questioned as it showed cross-reactivity against the acetylated H4 N-terminal tail and H3K9ac peptides [51-52]. In contrast, our antibody does not show any strong cross-reactivity against H3K9ac or tetra-acetylated H4 peptides (Figure 1C).

We readily detected a single H3K4ac band in immunoblots of extracts prepared from wild-type (WT) *S. cerevisiae* cells (Figure 1D). Importantly, there was no H3K4ac signal in extracts from cells that express either H3-K4R or H3-K4Q as the only source of H3 (Figure 1D). We also confirmed the presence of H3K4ac by mass spectrometry (MS). Histones were isolated from exponentially growing yeast cells (Figure 1E). After trypsin digestion, histone peptides were analysed by nano-LC MS/MS. In histones purified from wild-type cells, we identified a doubly charged precursor ion with the expected mass-to-charge ratio (m/z) for the tryptic peptide 3-TKacQTAR-8. The m/z ratio for the monoisotopic form of this precursor ion was determined with high accuracy as 373.7113 (Figure 1F). The experimental mass of the non-protonated peptide corresponding to this precursor ion (745.4070 Da) was in excellent agreement (−1.6 ppm) with the theoretical mass expected for a K4-acetylated peptide (745.4082 Da) and clearly different from the predicted mass of a peptide containing trimethylated K4 (745.4592 Da). Fragmentation of this precursor peptide by collision-activated dissociation resulted in *b*- and *y*-type ion series (Figure 1G) with diagnostic fragment ions (*e.g.* the mass difference between the *y3* and *y5* fragments and the mass of the *b2* fragment) that unambiguously proved the presence of an acetyl group on H3K4. However, technical limitations precluded us from determining the abundance of H3K4ac by MS. Using synthetic peptides, we found that the tryptic peptide containing H3K4ac was extremely poorly retained during reverse phase HPLC. Because of this we were not able to accurately assess the stoichiometry of H3K4 acetylation.

To investigate the presence of H3K4ac in chromatin, we performed chromatin immunoprecipitation (ChIP) in strains expressing either H3-WT or H3-K4R. Our initial screen of various genomic regions by qPCR revealed a strong enrichment of H3K4ac (relative to ChIP of non-modified H3) at some gene promoters (*MAE1*, *PHO85*, *RPL25*) a modest enrichment at other genes (*BNA5*, *MCM1*, *BAP2*, *BAP3*) and a very low enrichment at a region ~1 Kb from telomere III-R (*TEL03R*) (Figure 1H). These results are consistent with our genome-wide ChIP-chip data showing an enrichment of H3K4ac in euchromatin at the promoters of highly transcribed genes (see below). We performed control experiments to confirm the target lysine specificity of our antibody in ChIP assays. The ChIP signal obtained with the H3K4ac antibody dropped significantly at all regions tested in the *H3-K4R* strain (Figure 1H). As an average for all the promoters tested, the signal obtained by ChIP with our H3K4ac antibody in the *WT* strain is about 7-fold higher than the non-specific signal (noise) derived from the *H3-K4R* strain. The average signal-to-noise ratio increases to 9-fold when considering only the four promoters where the signal is most abundant in *WT* cells. Certain promoters show a higher background, such as the *RPL25* promoter (3-fold signal-to-noise), which may reflect some degree of non-specific binding of

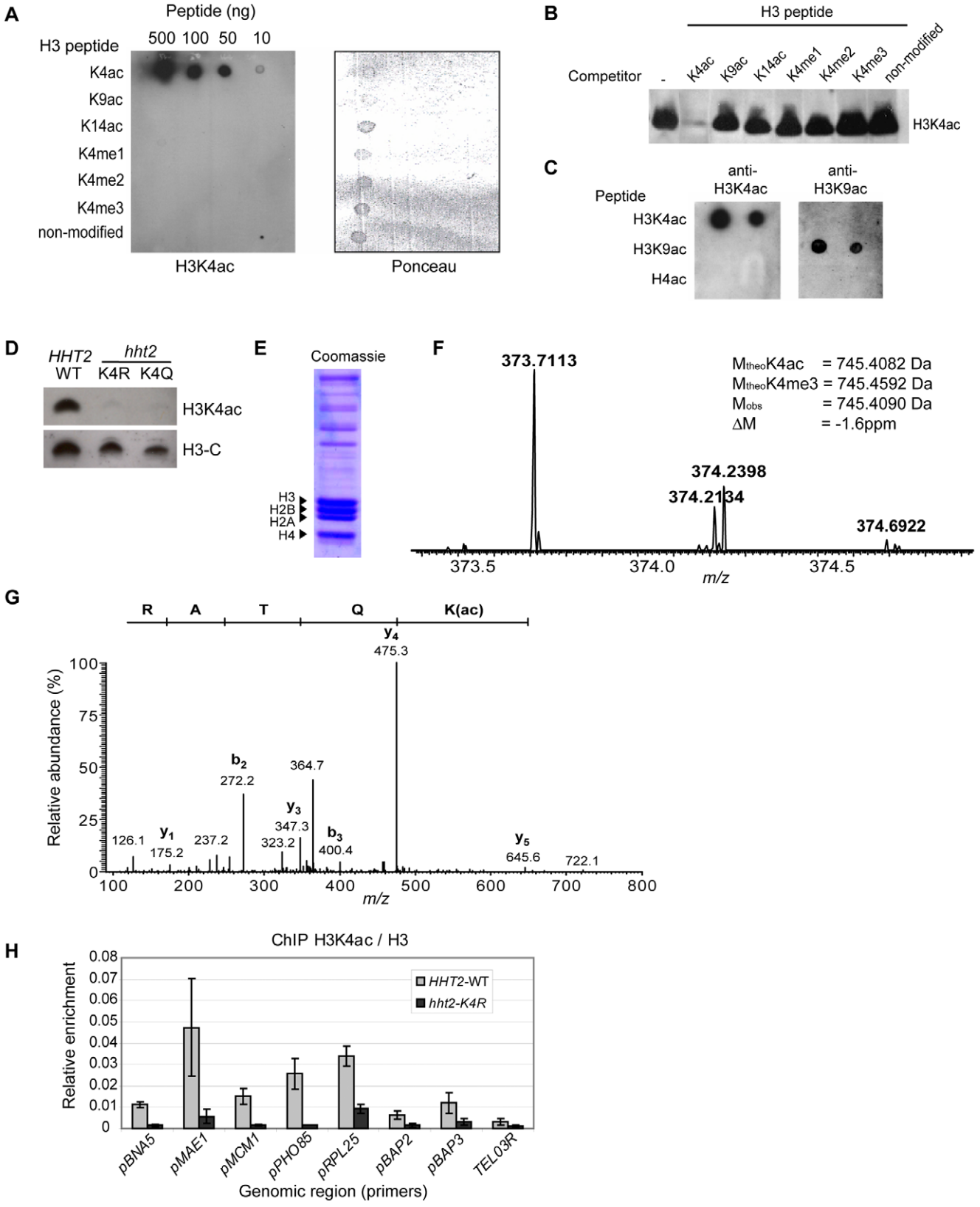

Figure 1. H3K4 Is Acetylated in *S. cerevisiae*. (A) Synthetic peptides derived from the histone H3 N-terminal tail (residues 1 to 10) with modifications at different residues were applied to a nitrocellulose membrane. The membrane was incubated with the H3K4ac antibody, a horseradish peroxidase-conjugated anti-rabbit IgG, and signals visualised by chemiluminescence (left). Ponceau S staining showing that all the peptides bound to nitrocellulose (right). (B) Immunoblots carried out with nuclear extracts from mouse thymocytes. The membrane was cut into strips and incubated with H3K4ac antibody that was pre-incubated with the indicated competitor peptides (1 μg/ml), resulting in a molar ratio of

approximately 1000:1 (peptide:antibody). (C) Dot blots of synthetic peptides (100ng each) containing H3K4ac, H3K9ac, and tetra-acetylated histone H4, (K5, 8, 12, 16)ac, were incubated with H3K4ac and H3K9ac antibodies. Antibody binding was detected as described above. (D) Whole-cell lysates from strains expressing either WT or mutant versions of H3 were analysed by immunoblotting for H3K4ac or a non-modified C-terminal peptide of H3. (E) Coomassie stained gel of histones purified from exponentially growing yeast cells. (F) Doubly charged precursor ion with the expected *m/z* ratio for tryptic peptide 3-TKacQTAR-8. The experimental and theoretical masses of the non-charged peptides are indicated in the inset along with the mass difference between the empirically determined and the predicted mass of the K4-acetylated peptide. (G) MS/MS spectrum of the doubly charged precursor ion with *m/z* 373.7113. The peptide sequence is shown from its C-terminus to its N-terminus above the spectrum. (H) Chromatin immunoprecipitation (ChIP) assays were analysed by quantitative PCR to determine the abundance of H3K4ac relative to non-modified H3 ChIP at different loci in WT and *H3-K4R* cells.
doi:10.1371/journal.pgen.1001354.g001

our H3K4ac to other acetylated lysine residues present in proteins in the vicinity of the *RPL25* promoter. Nevertheless, our H3K4ac-specific enrichment values are comparable with previously published ChIP data using acetyl-lysine specific antibodies, where the signal-to-noise ratio ranged from 3 to 10-fold [53]. These results validate the specificity of our antibody in ChIP assays and confirm the presence of H3K4ac in gene promoters.

H3K4 acetylation depends upon *GCN5* and *RTT109*

To screen for potential HATs that act on H3K4, we monitored H3K4ac by immunoblotting extracts derived from strains carrying gene disruptions of previously identified HATs. Using this approach, we found that *GCN5* and *RTT109* were required for H3K4ac *in vivo* (Figure 2A, lanes 4 and 7). Consistent with a recent report [54], *gcn5*Δ and *rtt109*Δ single mutants also exhibited lower levels of H3K9ac than WT cells (Figure 2A). A *gcn5*Δ *rtt109*Δ double mutant showed levels of H3K4ac comparable to the background observed in histones from *H3-K4R* cells (Figure 2B, 2C), suggesting that, as is the case for H3K9ac, *GCN5* and *RTT109* are responsible for essentially all H3K4ac in yeast.

H3K4 deacetylation is dependent upon *HST1* and *SIR2*

To identify potential HDACs responsible for H3K4 deacetylation we repeated our immunoblotting screen with extracts from different HDAC deletion mutants. This revealed that H3K4 deacetylation is, at least in part, dependent upon *HST1* and *HDA1* (Figure 2D, lanes 2 and 7). Deletion of *HDA1* also led to an increase in H3K9ac, whereas the *hst1*Δ mutant showed an increase in H3K4ac but not H3K9ac (Figure 2D, bottom panel). Because of this, we focussed our experiments on Hst1. *S. cerevisiae* Hst1 is a member of a family of five NAD^+-dependent HDACs, known as sirtuins because of their homology to Sir2. These enzymes are readily inhibited by nicotinamide, one of the products of the deacetylation reaction. Consistent with this, exposure of WT cells to nicotinamide caused an increase in H3K4ac (Figure S1). Treatment of *hst1*Δ cells with nicotinamide led to a further increase in H3K4ac (Figure S1), which suggested that other sirtuins also contribute to H3K4 deacetylation. We analysed H3K4ac in a collection of sirtuin double mutants and found that deletion of *SIR2* in cells lacking Hst1 increased H3K4ac above the levels observed in WT cells and *hst1*Δ single mutants (Figure 2E, 2F, lanes 1-3). This suggests that *SIR2* can compensate for the loss of *HST1* for global deacetylation of H3K4. In *S. cerevisiae*, Sir2 promotes heterochromatin formation through histone deacetylation in specific chromosomal regions, namely the silent mating type loci (*HMR***a** and *HML*α), sub-telomeric regions and a subset of ribosomal DNA (rDNA) repeats [55]. By immunoblotting whole-cell extracts, we found no global increase in H3K4ac in a *sir2*Δ single mutant (Figure 2D, lanes 1 and 11). We hypothesised that, in WT cells, Sir2 might deacetylate H3K4 mainly at heterochromatic loci, which represent a relatively small fraction of the genome. To test this hypothesis, we performed ChIP in WT, *hst1*Δ, *sir2*Δ and *hst1*Δ *sir2*Δ double mutant cells at different euchromatic and heterochromatic regions known to be deacetylated by Hst1 and Sir2 respectively: the promoters of *BNA5* and *BTN2*, targeted by Hst1 [56], a sub-telomeric region (*TEL03R*) and the silent mating type *locus HML*α, targeted by Sir2 [55]. We also analysed an origin of replication (*ARS1233*) and the *BSC1* gene promoter, which are not known to be targeted by either Sir2 or Hst1. The *sir2*Δ single mutation elevated H3K4ac at the *TEL03R* and *HML*α heterochromatic loci to levels comparable to those observed in the *hst1*Δ *sir2*Δ double mutant (Figure 2G). The deletion of *HST1* had virtually no effect at these regions. We therefore conclude that H3K4 deacetylation in heterochromatic regions is solely dependent upon *SIR2*. Conversely, deletion of *HST1* increased H3K4ac at the promoters of *BNA5* and *BTN2*, but not at other euchromatic regions (Figure 2G). The *SIR2* deletion affected H3K4ac only slightly at those loci whereas the *hst1*Δ *sir2*Δ double mutant showed higher levels of H3K4ac than in any of the single mutants (Figure 2G). This is consistent with a previous study [57] and suggests that Sir2 can also contribute to deacetylate H3K4 at Hst1-targeted loci.

Genome-wide presence of H3K4ac in euchromatin and active promoters

To localise H3K4ac throughout the genome, DNA recovered from ChIPs was analysed with high-resolution tiling arrays (Affymetrix 1.0R). Nucleosome density was controlled by normalising H3K4ac to the results of a ChIP experiment performed from the same cell lysates using an antibody against the non-modified C-terminal tail of H3 (H3-C).

The data showed that H3K4ac peaks are distributed along all chromosomes and relatively low levels of H3K4ac are observed at most sub-telomeric regions (Figure S2). This is most apparent on chromosome III, where H3K4ac is markedly depleted in large sub-telomeric regions that encompass *HML*α and *HMR***a** (Figure S2), where Sir2 was previously shown to promote histone deacetylation. Closer manual inspection of the results using the UCSC genome browser [58] indicated that the strongest peaks of H3K4ac are located at highly transcribed genes, such as ribosomal protein genes. Two examples (*RPL37A* and *RPS31*) are highlighted in Figure 3A. We performed a systematic analysis aimed at determining whether H3K4ac was generally enriched at promoters. For this purpose, we aligned H3K4ac data derived from genes with upstream intergenic regions (IGRs) that contain divergent promoters. Based on this criterion, these IGRs are devoid of DNA sequences corresponding to 3′-untranslated regions (3′-UTRs) and transcriptional termination sequences. This analysis revealed that H3K4ac peaks slightly upstream of the 5′-ends of genes (Figure 3B). Furthermore, the degree of H3K4ac enrichment correlated with transcriptional activity (as measured in [59]). For the most highly transcribed genes (50+ mRNA/hr), H3K4ac peaks upstream and appears to spread into coding regions (Figure 3B). In less frequently transcribed genes, H3K4ac also peaks just upstream of 5′ends, but sharply drops in coding regions (Figure 3B). We performed a similar analysis for genes that have converging 3′-ends. The corresponding IGRs contain

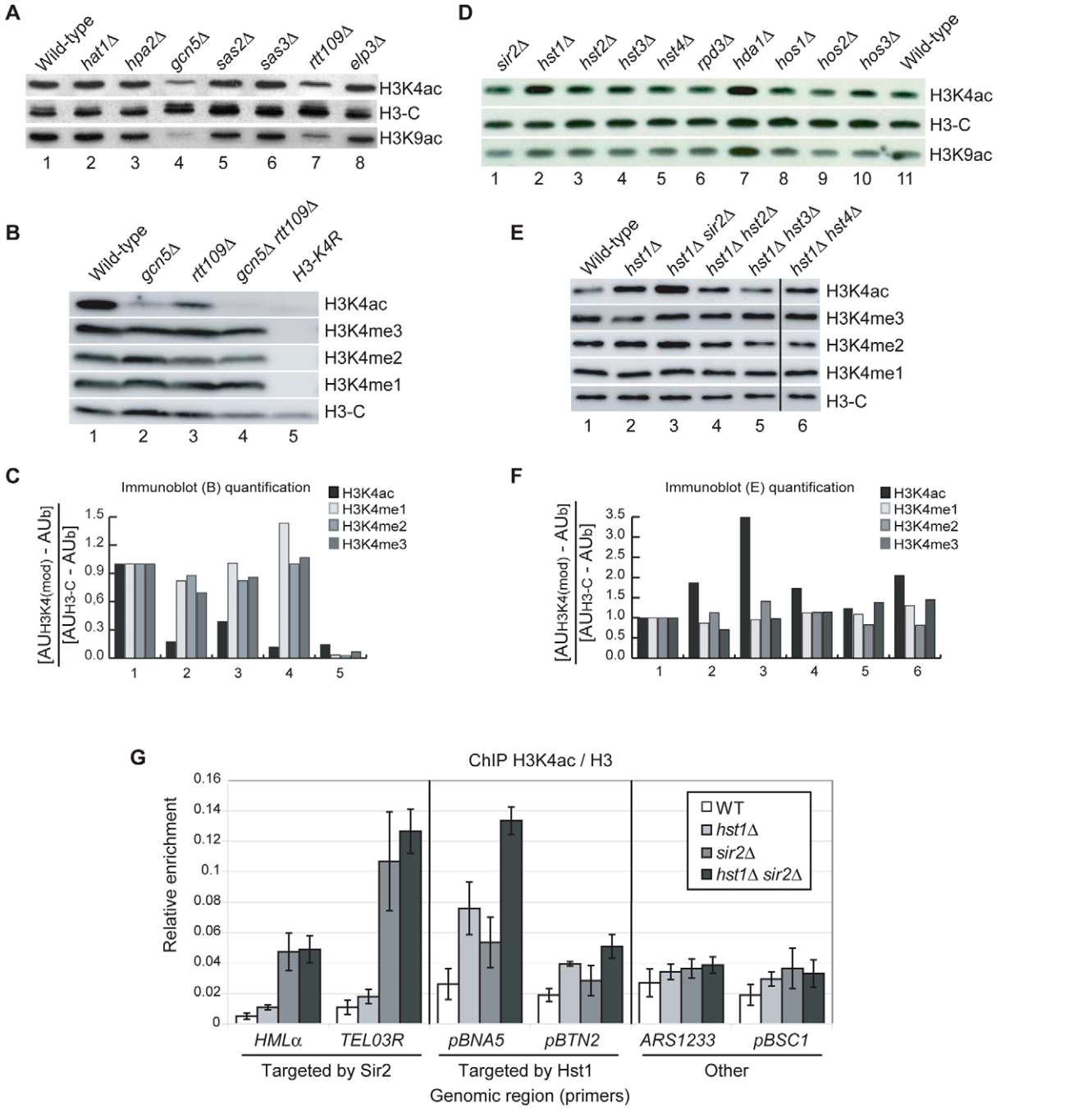

Figure 2. HATs and HDACs That Contribute to H3K4ac *In Vivo*. (A–B) Whole-cell lysates prepared from strains with deletions of known HAT encoding genes were analysed by immunoblotting with the indicated antibodies. (C) Quantification of the immunoblots shown in (B). Signals for each band were expressed in Arbitrary Units (AU) and, after background subtraction (AUb), normalised to the H3-C signal measured in each strain. (D–E) Whole-cell lysates obtained from strains with deletions of known HDAC encoding genes were analysed by immunoblotting with the indicated antibodies. (F) Quantification of the immunoblots shown in (E), calculated as described above. (G) Chromatin immunoprecipitation (ChIP) was performed by quantitative PCR to determine the abundance of H3K4ac at different loci in WT, *hst1*Δ, *sir2*Δ or *hst1*Δ *sir2*Δ strains. The six target regions were divided into three groups: regions targeted by Sir2, gene promoters targeted by Hst1 and other gene regions not targeted by Sir2 or Hst1. The *TEL03R* primers amplify a portion of *ARS319*, a unique sequence region approximately 1 Kb from the telomeric repeats on the right arm of chromosome III. Results are expressed as a ratio of ChIP signals obtained from the same extracts with antibodies against H3K4ac and a non-modified H3 C-terminal peptide.
doi:10.1371/journal.pgen.1001354.g002

3′-UTRs and transcriptional termination sequences, but are devoid of promoters. These chromosomal regions revealed only a modest enrichment for H3K4ac in the most highly transcribed gene group (Figure 3C, coordinates 0.0 and beyond). This effect probably results from the aforementioned spreading of H3K4ac peaks over the whole body of highly transcribed genes (compare

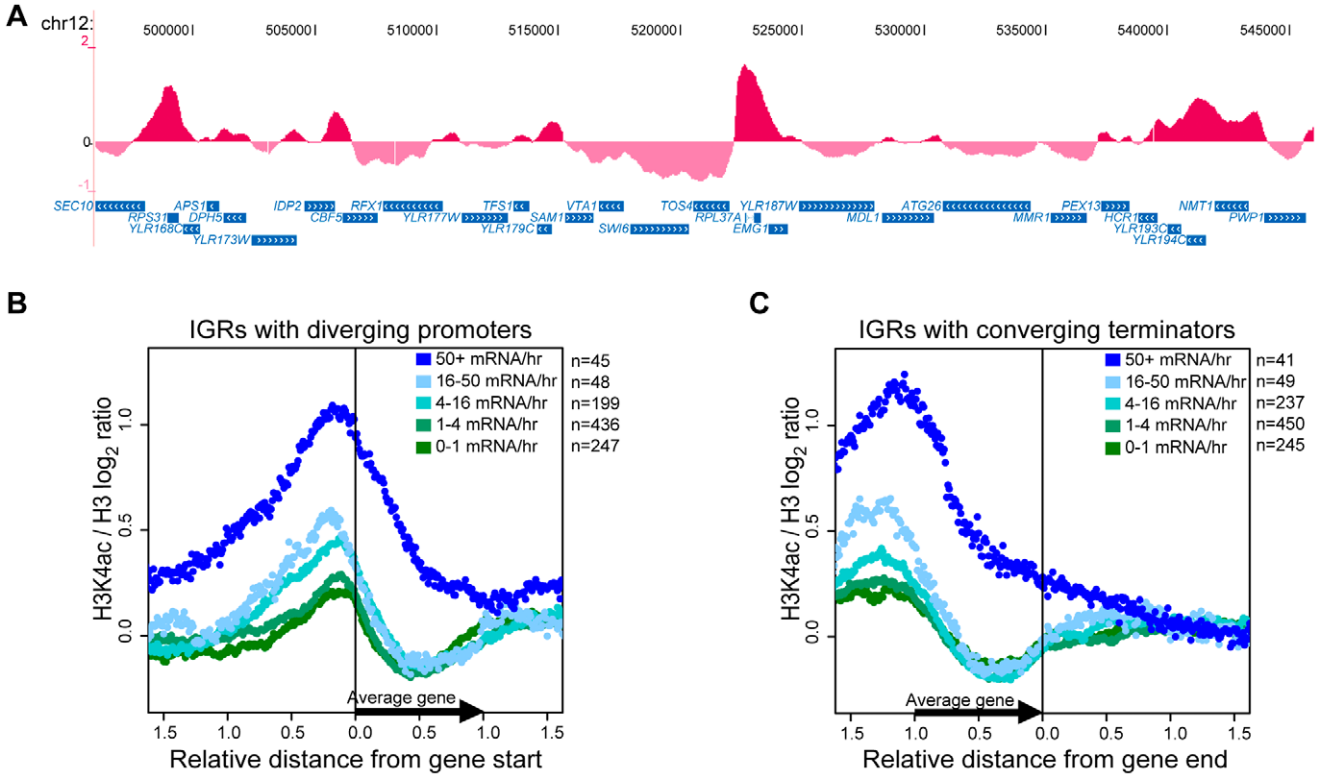

Figure 3. H3K4ac Is Enriched at Promoters of Transcribed Genes. (A) Examples of the localisation pattern of H3K4ac along a 50 kb segment of chromosome 12, as displayed on the UCSC genome browser (http://genome.ucsc.edu/) [58]. The data (purple) are represented as a $\log_2$ ratio of H3K4ac over non-modified H3 C-terminus ChIP signals and represent the average of 3 biological replicates. The names, position and orientation of ORFs (*S. cerevisiae* assembly Oct. 2003) are shown (blue) at the bottom of each panel. (B–C) Systematic analyses of the genome-wide location of H3K4ac / H3-C ChIP signals at: (B) 5′-ends of ORFs with divergent promoter regions. (C) 3′-ends of ORFs with convergent terminator regions. The data was aligned to the closest 5′- or 3′-end of ORFs, normalised for gene length and sub-divided into 5 groups according to transcriptional activity (mRNA/hr) [59]. For simplicity, the relative position value for each data point was rounded to the nearest hundredth. The *y*-axes show the abundance of H3K4ac (average of three biological replicates) as a function of relative position along the nearest gene (*x*-axes).
doi:10.1371/journal.pgen.1001354.g003

Figure 3B and 3C). From this data, it is clear that H3K4ac peaks at gene promoters and the degree of enrichment is proportional to the rate of transcription.

H3K4ac is upstream of H3K4me3 at gene promoters

We found that H3K4ac was enriched at transcriptionally active promoters (Figure 3B) and it has been reported that H3K4me3 is also present at this location in active genes [20]. To explore the relationship between H3K4ac and H3K4me, we compared our genome-wide H3K4ac localisation data with the previously published high-resolution data for H3K4me1, -me2 and -me3 [60]. Strong peaks of H3K4ac were generally located upstream of H3K4me3 in gene promoters, followed by the typical pattern of H3K4me2 and H3K4me1 enrichment along coding regions (Figure 4A and more examples in Figure S3). There is a considerable overlap between H3K4ac with H3K4me3, although their localisation patterns are not identical. We repeated the H3K4me3 ChIP-chip under our conditions (as described for H3K4ac) and our results (data not shown) produced an enrichment pattern nearly identical to the Kirmizis et al. dataset [60]. Systematic analysis showed that H3K4me3 spreads further into coding regions than H3K4ac in moderately and highly transcribed genes (from 4 to 50+ mRNA/hr) (Figure 4B). The peak intensity for the H3K4ac signals are slightly upstream of H3K4me3 (Figure 4B), which is consistent with the UCSC track observations (Figure 4A).

To investigate whether this pattern was evolutionarily conserved, we examined the localisation of H3K4 modifications in human $CD4^+$ lymphocytes from previously published ChIP-seq data [19,51]. Manual inspection of the data with the UCSC genome browser revealed H3K4ac and H3K4me3 overlapping at many transcriptional start sites, but H3K4ac was slightly upstream of H3K4me3 (representative examples are shown in Figure S4). Interestingly, H3K4ac peaks also overlap with RNApol II more closely than H3K4me3 at these genes (Figure S4), suggesting a function for H3K4ac in transcriptional regulation in human cells. From these data, we conclude that H3K4ac is present at transcribed gene promoters, and is adjacent to a unidirectional gradient of H3K4me3, -me2 and -me1 that proceeds from promoters into coding regions. This pattern of H3K4 modifications has been conserved during evolution.

Genome-wide overlap of H3K4ac and H3K4me3 at promoters

To investigate and compare the proportion of promoters that are enriched in H3K4ac or H3K4me3, we transformed the log-ratio data into Z-scores (see Materials and Methods). This was performed to normalise datasets with different scales, thus allowing a direct comparison of the H3K4ac and H3K4me3 datasets. We then established a threshold value above which a promoter was judged enriched in H3K4ac or H3K4me3 relative to H3. When the cut-off was set at the 90^{th} percentile (only promoters with

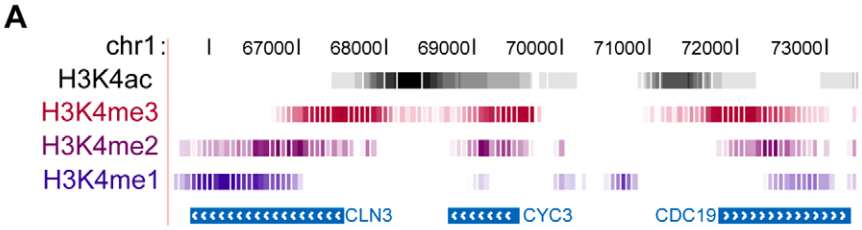

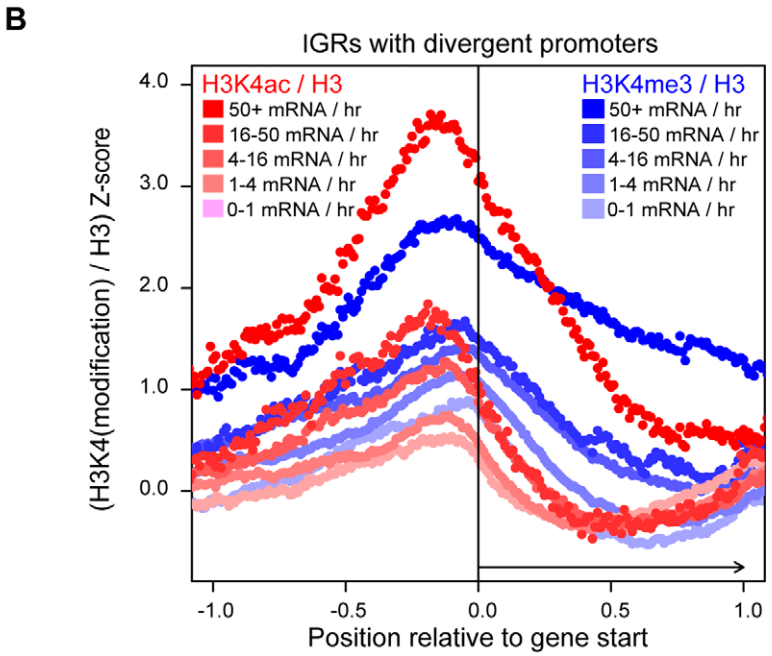

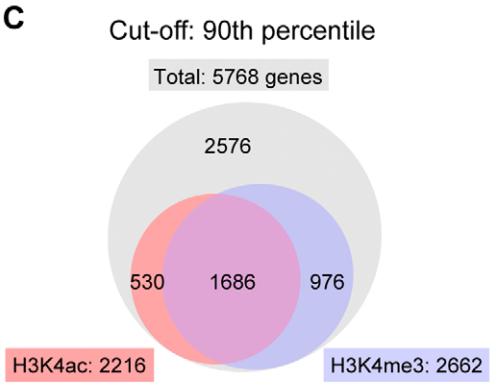

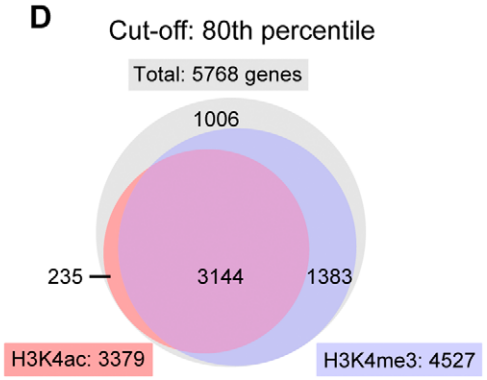

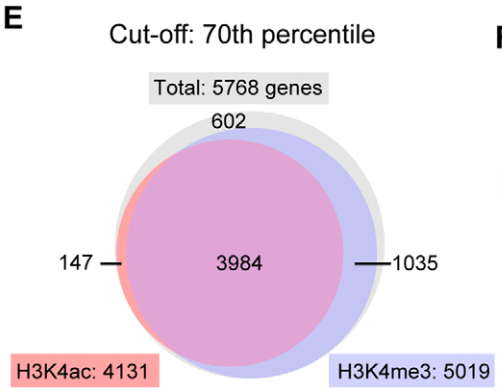

F

	Cut-off			
	90th	80th	70th	
H3K4ac	38%	59%	72%	% of total promoters
H3K4me3	46%	78%	87%	
H3K4ac + H3K4me3	76%	93%	96%	% of promoters enriched for H3K4ac
	63%	69%	79%	% of promoters enriched for H3K4me3

Figure 4. H3K4ac Is Located Upstream of H3K4me3. (A) The H3K4ac / H3 (black) ChIP-chip data were aligned with the H3K4me3 (burgundy), -me2 (purple) and -me1 (blue) data from [60] and displayed in the UCSC genome browser (http://genome.ucsc.edu/). Each vertical line represents one probe in the dataset and the intensity of the color is proportional to the enrichment of the modification. For clarity, only the probes with a $\log_2$ ratio above 0 are shown for each dataset. (B) Systematic alignement of H3K4ac / H3 (red shades) and H3K4me3 / H3 (blue shades) ChIP-chip data at intergenic regions (IGRs) with divergent promoters (as in Figure 3B). The raw ChIP-chip data were converted into Z-scores in order to be compared on the same scale (see Material and Methods). (C–E) Venn diagrams illustrating the overlapping number of promoters that are enriched for H3K4ac or H3K4me3. The cut-off indicates the H3K4(mod) / H3-C Z-score threshold at which a given promoter was judged to be enriched in either H3K4ac or H3K4me3. For example, with a cut-off at the 90th percentile (C), the red circle contains the number of promoters that have H3K4ac / H3 signal ratios in the top 10% of the genome. (F) A table displaying the data from the Venn diagrams as percentages.
doi:10.1371/journal.pgen.1001354.g004

enrichment values scoring in the top 10% of all values), H3K4ac was found to be enriched at 38% of all gene promoters, whereas H3K4me3 was enriched at 46% of promoters (Figure 4C and 4F). Of the promoters enriched in H3K4ac, 74% were also enriched in H3K4me3. This value increased to 93% when the cut-off was set to the top 80th percentile (Figure 4D and 4F) and 96% at the top 70th percentile (Figure 4E and 4F), indicating that most promoters enriched in H3K4ac also have a significant enrichment in H3K4me3. However, a smaller proportion of H3K4me3-enriched promoters also contain H3K4ac: 63%, 69% and 79% for the top 90th, 80th and 70th percentile cut-offs respectively (Figure 4F). From this we conclude that, genome-wide, H3K4me3 is enriched at a greater number of promoters than H3K4ac, and that most promoters which harbour H3K4ac are also enriched in H3K4me3.

Set1-mediated H3K4me2 and me3 limit the accumulation of H3K4ac

Since H3K4ac and H3K4me3 overlap considerably at the promoters of many genes, we sought to determine if there is a competition for the lysine 4 substrate. Based on mass spectrometry, we found that a *SET1* deletion caused a global increase in H3K4 acetylation (Figure 5A). This result was corroborated by immunoblotting data showing that H3K4ac, but not H3K9ac was elevated in *set1*Δ cells (Figure 5B, 5C). The immunoblotting result truly reflected an increase in H3K4ac in *set1*Δ cells, rather than cross-reaction to other sites of acetylation, because no signal was observed in *set1*Δ *H3-K4R* mutant cells (Figure 5D). In addition, an H3K4ac peptide, but not H3K9ac or non-modified K4 peptides, could compete the signal observed with the K4ac antibody in WT and *set1*Δ cells (Figure 5E). Set1 is part of COMPASS, a complex that has multiple subunits which contribute to the different degrees of H3K4 methylation (me1, me2 or me3) [61-63]. To determine which subunits of COMPASS were important to limit the accumulation of H3K4ac, we performed immunoblots using strains with single gene deletions of all the COMPASS subunits. Cells lacking *SET1*, *BRE2*, *SDC1*, *SWD3* or *SWD1* have in common a complete absence of H3K4me2 and me3, but mutations of these genes differentially affect H3K4me1 (Figure 5F). For instance, *bre2*Δ and *sdc1*Δ mutants have WT levels of H3K4me1 (Figure 5F, lanes 1, 3 and 5), whereas *set1*Δ, *swd3*Δ and *swd1*Δ mutants lack all forms of H3K4me (lanes 2, 6 and 8). Nonetheless, relative to WT cells, all these mutants increased H3K4ac to similar degrees (Figure 5F, compare lane 1 with lanes 2, 3, 5, 6 and 8). An *spp1*Δ mutant with nearly normal levels of H3K4me2, but reduced H3K4me3 showed a moderate increase of H3K4ac (Figure 5F, lanes 1 and 7). In striking contrast, an *shg1*Δ mutant that retained normal levels of H3K4me2 and H3K4me3 did not show a significant increase in H3K4ac compared with WT cells (Figure 5F, lanes 1 and 4). These results argue that the increase in H3K4ac observed in several mutants of the COMPASS complex occurs mainly because of the absence of H3K4me2 and me3, rather than a lack of H3K4me1.

Since a global reduction in H3K4me2 and me3 led to an increase in H3K4ac, we wished to investigate if the opposite was also true. Immunoblots of cell lysates prepared from *gcn5*Δ and *gcn5*Δ *rtt109*Δ strains, with strongly reduced H3K4ac, showed no significant increase in any form of H3K4me (Figure 2B, 2C). Conversely, we observed no apparent decrease in H3K4me1, me2 or me3 in cells with elevated levels of H3K4ac (*hst1*Δ or *hst1*Δ *sir2*Δ, (Figure 2E, 2F). Therefore, although H3K4ac increases in mutant cells lacking H3K4me2 and me3, changes in H3K4ac do not influence global levels of H3K4 methylation. These results suggest that the relative abundance of H3K4ac does not merely reflect a simple competition for the H3K4 substrate.

Set1 regulates H3K4ac at promoters and the 5′ end of coding regions

To see if the deletion of *SET1* led to a change in the genome-wide distribution of H3K4ac, we performed ChIP-chip experiments to compare the localisation of H3K4ac in *set1*Δ and WT cells. Manual inspection of the data in the UCSC Genome Browser revealed changes in the distribution and the relative abundance of H3K4ac in *set1*Δ cells, at several gene promoters. For example, at the *FKH1* and *SUR7* genes, H3K4ac is increased at the promoter region and spreads towards the coding region in the *set1*Δ strain (Figure 5G, 5H). Systematic alignment of divergent promoter regions showed that the deletion of *SET1* led to a global increase in the relative abundance of H3K4ac at gene promoters (Figure 5I, blue versus black dots). We also observed a slight shift of H3K4ac towards the 5′ ends of the coding region in *set1*Δ cells (Figure 5I). To better assess the changes in localisation of H3K4ac in the *set1*Δ strain, the H3K4ac ChIP-chip data from WT cells were subtracted from those of *set1*Δ cells. This analysis clearly showed that the strongest difference in H3K4ac occurs at position 0 relative to gene start (Figure 5I, green dots), which corresponds to the 5′ ends of coding regions. The fact that the shoulder of the H3K4ac peak in the *set1*Δ strain is skewed over downstream sequences argues that this increase is not merely due to increased peak signal in *set1*Δ cells, since this would lead to a symmetric increase in each shoulder. Instead, this shows that, on average, H3K4ac spreads further into the 5′ ends of coding regions in *set1*Δ cells. We also observed a global decrease in H3K4ac at the 3′ ends of coding regions in *set1*Δ mutants (Figure 5I). The significance of this decrease is unknown. Nevertheless, we can conclude that the global increase in H3K4ac observed in *set1*Δ mutant cells by MS and immunoblotting occurs more prominently at the promoters and 5′ ends of coding regions relative to other regions.

The global average increase of H3K4ac in *set1*Δ cells likely occurs at a subset of genes and not all genes. Manual inspection of the datasets clearly shows that the H3K4ac pattern remains unaffected at certain genes, for example *GAL80* and *YML053c* (Figure 5H). To provide further evidence that the increase in H3K4ac observed in the *set1*Δ strain did not occur equally at all genes, we performed ChIP-qPCR experiments in WT and *set1*Δ strains at three genes: *CPA2*, *ARG7* and *FKH1*. These genes were selected because they respectively showed little, moderate and

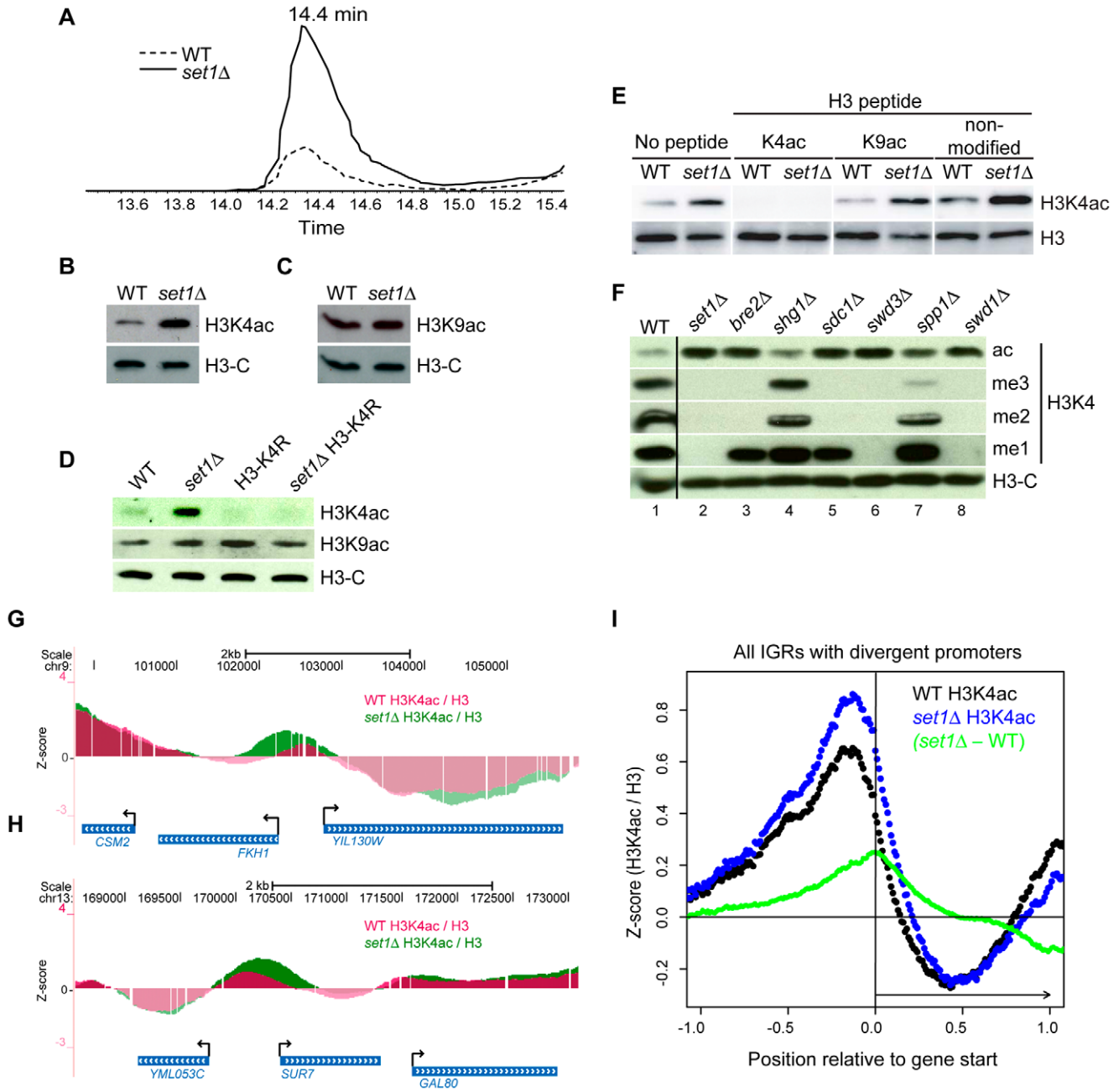

Figure 5. The COMPASS Complex Limits Global Levels of H3K4ac and Confines H3K4ac Localisation to Promoter Regions. (A) Extracted ion chromatogram showing the retention time of peptide 3-TKacQTAR-8 during reverse phase HPLC and its relative abundance in WT and *set1*Δ cells. (B–F) Whole-cell lysates from the indicated mutants were analysed by immunoblotting. In (E), a peptide competition assay was performed as described in Figure 1B. (G–H) Examples of the localisation pattern of H3K4ac in either WT (purple) or *set1*Δ (green) strains at two genomic regions displayed using the UCSC genome browser (genome.ucsc.edu) [58]. The data represents the normalised (Z-score) $\log_2$ ratio of H3K4ac over H3-C (see Materials and Methods). (I) Systematic analyses of H3K4ac in WT versus *set1*Δ cells in all intergenic regions (IGRs) that contain divergent promoters. The raw H3K4ac ChIP-chip data in WT or *set1*Δ cells were normalised either against their respective H3-C ChIP (black: WT, blue: *set1*Δ), converted into Z-scores (see Material and Methods) and aligned relative to the 5′-end of the corresponding ORF (normalised as described in Figure 3). The difference between the *set1*Δ and WT datasets (*set1*Δ - WT, green) is also shown.
doi:10.1371/journal.pgen.1001354.g005

large changes in H3K4ac in *set1*Δ strains according to our initial observations in the UCSC Genome Browser. Our ChIP-qPCR analyses confirmed the ChIP-chip results for H3K4ac in the *set1*Δ strain (Figure S5A-S5C). Therefore, although the absence of H3K4me2 and me3 leads to a global increase in H3K4ac (Figure 5A, 5B), ChIP assays demonstrate that the increase in H3K4ac is more prominent at some genes than others.

H3K4ac and gene expression

Since H3K4ac is enriched at highly transcribed gene promoters, we explored the possibility that H3K4ac might play a role in gene transcription. Genetic analysis of the function of H3K4ac is complicated by the fact that mutation of H3K4 abolishes both acetylation and methylation. To circumvent this problem, we compared the global mRNA profile of a *set1*Δ strain, which lacks

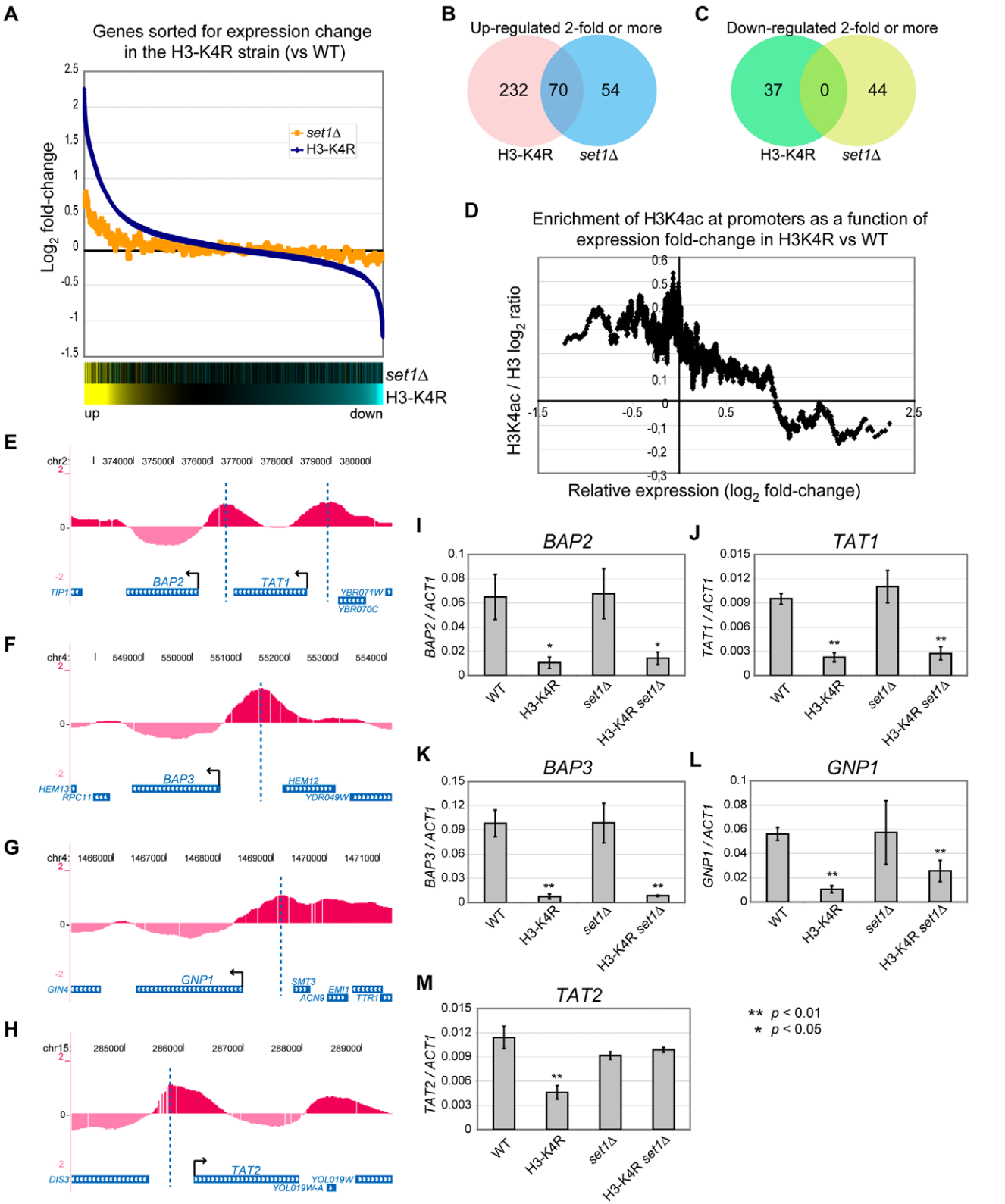

Figure 6. Global mRNA Expression Profiles of *set1*Δ and *H3-K4R* Mutant Strains. (A) Graph of mRNA expression fold-change relative to WT cells in the *H3-K4R* (blue) and *set1*Δ (yellow) strains for all the analysed genes. The genes were ranked according to $\log_2$ fold-change in the *H3-K4R* strain and a sliding average (window = 50, step = 1) was applied to the data on the *y*-axis. The bottom panels are heat map illustrations of the $\log_2$ fold-change, where yellow indicates an increase in mRNA abundance in the mutant strains relative to WT cells and blue indicates a decrease. (B–C) Venn diagrams showing the overlap between groups of genes up-regulated (B) or down-regulated (C) at least two-fold when either the *H3-K4R* or the *set1*Δ strain is compared with WT cells. (D) Graph of the H3K4ac / H3 ratio at the promoter regions of each gene (average for from −200 to +1bp relative to the start codon) derived from the ChIP-chip data as a function of their $\log_2$ fold-change in mRNA abundance in the *H3-K4R* mutant strain

versus WT cells (derived from the mRNA expression microarray data). A sliding window average was applied to the data on both axes (window = 50, step = 1). (E–H) Localisation of H3K4ac near genes that belong to the ontology group of "amino acid transporters" and are poorly expressed in *H3-K4R* mutants compared with WT cells: (*BAP2*/YBR068C, *TAT1*/YBR069C, *BAP3*/YDR046C, *GNP1*/YDR508C, *TAT2*/YOL020W). The start sites of these genes are indicated by arrows and vertical dashed lines indicate the peaks of H3K4ac in their upstream regions. The display is from the UCSC genome browser (http://genome.ucsc.edu/). (I–M) RT-qPCR analyses of RNA extracted from the indicated strains (WT, *H3-K4R*, *set1*Δ, *H3-K4R set1*Δ). The values were normalised to *ACT1*. The data represent an average of three biological replicates.
doi:10.1371/journal.pgen.1001354.g006

H3K4me but retains H3K4ac, with that of an *H3-K4R* mutant where both H3K4 acetylation and methylation are lost. In order to get a global view of the expression profiles in both mutants, we ranked the genes by $\log_2$ fold change in mutant strains relative to WT cells (Figure 6A). At one end of the spectrum, we found many genes that are up-regulated in both the *H3-K4R* and the *set1*Δ mutant strains (Figure 6A, left part). Many of these genes are up-regulated only in *H3-K4R* mutant cells (Figure 6A, 6B). One possibility is that expression of some of these genes may be affected simply because of the lysine-to-arginine mutations, rather than a lack of modification. However, there is considerable overlap between the genes up-regulated in *H3-K4R* and *set1*Δ mutant strains (Figure 6B). We conclude that the repressed state of these genes in WT cells is likely to be dependent on H3K4me, rather than H3K4ac. This is consistent with previous reports showing a repressive function for *SET1* [64-66].

At the other end of the spectrum, we found a group of genes which were down-regulated in the *H3-K4R* strain, but were unaffected in the *set1*Δ strain (Figure 6A, right part), suggesting a positive role for H3K4ac in the expression of these genes. We identified 37 genes that were down-regulated 2-fold or more in the *H3-K4R* strain and 44 in the *set1*Δ strain. Strikingly, there was no overlap between these two groups of genes (Figure 6C), suggesting a function of H3K4 in gene expression that is independent of methylation. We next compared the H3K4ac abundance at promoter regions in WT (from our ChIP-chip dataset) with the expression change of the gene in the *H3-K4R* strain. The genes that are down-regulated in the *H3-K4R* strain have high levels of H3K4ac at their promoters in WT cells (Figure 6D), which is consistent with a direct role of H3K4ac in gene expression. Gene ontology term enrichment analysis of the genes down-regulated 2-fold or more in the *H3-K4R* strain, but whose expression was not affected in a *set1*Δ strain, identified genes encoding amino acid transporters ($p = 1.42 \times 10^{-5}$): *BAP2*/YBR068C, *TAT1*/YBR069C, *BAP3*/YDR046C, *GNP1*/YDR508C, *TAT2*/YOL020W. Inspection of our ChIP-chip data for these genes confirmed that they all had high levels of H3K4ac at their promoters in WT cells (Figure 6E-6H). We confirmed by RT-qPCR that these genes are down-regulated in an *H3-K4R* strain, but unaffected in a *set1*Δ strain (Figure 6I-6M). In contrast to the other RNAs that we monitored, the expression of the *TAT2* RNA was unexpectedly restored in a *set1*Δ *H3-K4R* double mutant strain, suggesting an indirect effect of the *SET1* deletion on this gene (Figure 6M). Taken together, our data suggest that H3K4ac has a positive and direct role in the transcription of a subset of yeast genes.

Discussion

Histone H3K4 methylation is an extensively studied modification in a wide range of organisms, and particularly in the budding yeast *Saccharomyces cerevisiae*. Using MS and highly specific antibodies we demonstrated that H3K4 is also acetylated in budding yeast. An earlier study of histone modifications had shown that both H3K4ac and H3K4me exist in human, mouse and ciliates [52] and, very recently, in *Schizosaccharomyces pombe* [67]. The versatility of genetic tools available in *S. cerevisiae*, and the ability to mutate histone H3K4, has enabled us to uncover a positive function for H3K4ac in the expression of a subset of genes that carry H3K4ac in their promoters. The presence of H3K4ac at active gene promoters has been conserved in human $CD4^+$ cells [51], which suggests a similar role for H3K4ac in gene expression in mammals. We also discovered that the COMPASS complex and H3K4me2 and me3 appear to globally limit the abundance of H3K4ac at promoters and its spreading into the 5′-coding regions of many genes.

Acetylation of the H3 N-terminal tail by specific HATs

Our targeted screen of known HAT-encoding genes has allowed us to identify *GCN5* and *RTT109* as responsible for H3K4ac *in vivo*. Gcn5 is the catalytic subunit of the ADA, SAGA, SLIK/SALSA transcriptional co-activator complexes [68] and has been highly conserved during evolution [69]. Our results are consistent with the fact that Gcn5 has been shown to acetylate multiple lysine residues within the H3 N-terminal tail [70-71] and is localised to active gene promoters dispersed throughout the genome [56]. Interestingly, *RTT109* is also important for the acetylation of H3K4. Furthermore, the *gcn5*Δ *rtt109*Δ double mutant has markedly less H3K4ac than the single mutants. Collectively, our results indicate that *GCN5* and *RTT109* promote H3K4ac via different pathways and/or in different contexts. If they were fully redundant, there should be no decrease in H3K4ac in the single mutants, which is not the case. However, we cannot exclude the possibility that they may also have partially redundant functions in mediating H3K4ac. *RTT109* encodes a HAT that mediates H3K56ac [72-75], which is involved in nucleosome assembly during DNA replication and the DNA damage response [76-78]. In addition, Rtt109 has recently been implicated in acetylating H3K9 and H3K27 *in vivo* and *in vitro* [54,79-80]. As is the case for H3K4ac, H3K9ac and H3K27ac are virtually undetectable by immunoblotting and mass spectrometry in *gcn5*Δ *rtt109*Δ cells [79]. Therefore, the same HATs are responsible for the bulk of both H3K4 and H3K9 acetylation.

H3 N-terminal tail acetylation and gene transcription

The genome-wide localisation pattern of H3K4ac showed strong peaks at the promoters of active genes. This enrichment has also been observed in the genome-wide patterns of other acetylated lysines in the H3 N-terminal tail, such as H3K9ac, H3K14ac and H3K18ac [20-21], suggesting that these modifications often occur together on chromatin. Our microarray analysis identified a relatively small group of genes (37 genes down-regulated by 2-fold or more, Figure 6C) that require H3K4ac, but not H3K4me, for normal expression. However, based on our ChIP-chip data, many other promoters contain high levels of H3K4ac. It is tempting to speculate that acetylation of H3K4 functions in a partially redundant manner with other sites of acetylation at many promoters to increase accessibility to the transcriptional initiation machinery and thereby facilitate gene expression. Interestingly, our gene ontology term analyses revealed a group of amino acid transporter genes (*BAP2*, *BAP3*, *TAT1*, *TAT2*, *GNP1*) that are co-regulated by levels of extracellular amino acids [81-84]. An interesting possibility is that the transcription factors involved in their expression require H3K4ac either alone

or in combination with other acetylated residues to specifically promote initiation of these genes.

Regional and functional specificity of *HST1* and *SIR2*

We identified a role for *HST1* in global deacetylation of H3K4 in euchromatin. *HST1* encodes a class III HDAC found in at least two complexes. Hst1 is part of a complex with Sum1 and Rfm1 [85-86]. Interestingly, the deletion of *SUM1* did not result in a significant global increase in H3K4ac based on immunoblotting (data not shown). Hst1 has also been found as a sub-stoichiometric subunit of the SET3 complex (SET3C) [87], which represses middle-sporulation genes during mitosis [88]. However, neither deletion of *HOS2* (encoding the main HDAC in the complex) (Figure 2C), nor that of any other components of SET3C led to a global increase in H3K4ac (data not shown). Our results suggest that Hst1 might act in a non-targeted manner to promote global deacetylation of H3K4. Alternatively, Hst1 might be part of another, as yet unidentified complex involved in H3K4 deacetylation.

Interestingly, we also observed some redundancy between *HST1* and *SIR2* for deacetylation of H3K4 in euchromatic regions. In specific conditions, Hst1 and Sir2 have been shown to act outside of the chromosomal regions where they "normally" exert their functions. For example, overexpression of *HST1*, but not *HST2* or *HST3*, can specifically compensate for the loss of silencing at *HMR***a** that occurs in a *sir2*Δ mutant [89]. Our results are also consistent with studies showing a strong connection between these two genes. Both genes share 71% identity in their sequence over 84% of the length of *HST1* [90]. *SIR2* was previously shown to affect the expression of euchromatic genes when *HTZ1* and *SET1* were deleted [91] and to interfere with the firing of a number of replication origins [92]. Moreover, studies of chimaeric proteins demonstrated that the N-terminal domains of Hst1 and Sir2 control the chromosomal location and function of both proteins. In contrast, other domains of Hst1 and Sir2 could be swapped, supporting the notion that these enzymes have similar substrate specificity [93]. We propose here that H3K4 is an important target for deacetylation by both Hst1 and Sir2. *HST1* and *SIR2* are both part of the same phylogenetic branch (subgroup Ia) of NAD^+-dependent HDACs (class III) that also includes human SIRT1 and *Drosophila* Sir2 [94], which are, therefore likely candidates for deacetylation of H3K4 in these organisms.

Patterns of mutually exclusive histone modifications

The relationship between H3K4ac and H3K4me differs from that of other modifications that occur on the same lysine residue. The best studied case is that of H3K9, which is either acetylated or methylated. H3K9ac and H3K9me are present at different genomic regions [51] and have opposing roles in transcriptional regulation. H3K9ac is found in promoter regions and stimulates transcription through the recruitment of TFIID [95], whereas H3K9me2 and me3 contribute to gene repression and pericentric heterochromatin structure by binding HP1 proteins through their chromo-domains [96-97]. In this case, deacetylation of H3K9 is essential for the establishment of H3K9 methylation [98-100]. Another example is H3K36ac and H3K36me3, which are respectively present in promoters and coding regions of transcriptionally active genes [101]. In contrast to these modifications, H3K4ac overlaps considerably with H3K4me3 in promoter regions. Furthermore, H3K4me2/me3 globally limit the levels of H3K4ac, which suggests the existence of mechanisms to establish the correct patterns of localisation of these mutually exclusive modifications. For example, H3K4me2/me3 could prevent H3K4ac from occurring in gene coding regions by simple competition for the H3K4 substrate. Another possibility is that H3K4 methylation might be a prerequisite step in a negative feedback loop that enables Hst1 to fine tune the levels of H3K4 acetylation in promoters and 5′-coding regions. Mechanisms that confine H3K4ac to some promoters may contribute to prevent spurious transcriptional initiation events [102] or attenuation of transcriptional initiation [66]. The potential to restrict the spreading of histone H3K4ac suggests a novel function for H3K4 methylation and reveals a previously unrecognised layer of chromatin regulation linked to the regulation of transcription *in vivo*.

Materials and Methods

H3K4ac antibody production and validation

Immunisation procedures and animal handling were carried out by Eurogentec. Sera from ten animals were screened prior to immunisation. Rabbits were immunised with the following peptide: ART(acetyl-K)QTARKSC. The efficiency of antibody production was monitored using ELISA. The antibody was affinity-purified using the same peptide coupled to a Sulfolink column (Thermo) and its specificity tested by dot blots with synthetic peptides and experiments where 1 μg/ml of the peptides were incubated with the antibody prior to immunoblotting.

Yeast strains and media

For most experiments, yeast strains were grown at 30°C in YPD (1% yeast extract, 2% peptone, 2% dextrose). A complete list of yeast strains is available in Table S1.

Whole-cell lysates and immunoblots

Yeast whole-cell lysates were prepared using an alkaline lysis protocol [103]. Essentially, 5×10^7 cells were resuspended in 500 μl of distilled water and 500 μl of 0.2 M NaOH was added. After 5 min at room temperature, cells were spun down, and resuspended in 100 μl SDS-PAGE sample buffer, boiled for 3 min and spun down again. About 7 μl (equivalent to 3.5×10^6 cells) of supernatant was typically loaded per lane and, after electrophoresis through an SDS-15% polyacrylamide gel, proteins were transferred to PVDF membranes using a semi-dry apparatus with in 29 mM Tris, 193 mM glycine, 0.02% SDS, 5% methanol for 2 h at 1 mA /cm^2 (set maximum:15 V). We used the following dilutions for antibody incubations: anti-H3K4ac: 1/500, anti-H3-C (AbCam ab1791 or home-made): 1/10 000, anti-H3K9ac (Millipore 07-539): 1/10 000, anti-H3K56ac (Millipore 07-677): 1/5000.

Histone sample preparation and mass spectrometry

Histones were acid extracted from *set1*Δ *hst1*Δ cells essentially as described previously [104], except that we added 100 mM sodium butyrate and 100 mM nicotinamide in the nuclear isolation buffer and wash buffers. H3 was purified and digested as previously described [105]. Intact core histones (approximately 10 μg of total protein acid extract) were separated using an Agilent 1200 HPLC system equipped with a fraction collector. Separations were performed using an ACE C_8 column (5 μm, 300 Å), 150×4.6 mm i.d., with a solvent system consisting of 0.1% trifluoroacetic acid (TFA) in water (v/v) (A) and 0.1% TFA in acetonitrile (v/v) (B). Gradient elution was performed from 5–70% B in 60 minutes at 0.7 ml/min. Fractions were collected in conical tubes in 60 second time slices. Individual histone peaks that eluted over multiple fractions were pooled together. Histone fractions were evaporated in a Speed-Vac. Dried fractions were resuspended in 0.1 M ammonium bicarbonate (without pH adjustment) and digested overnight at 37°C using 1 μg of trypsin. Samples were acidified

with 5% TFA in water (v/v) prior to LC-MS/MS analysis. Tryptic digests of histone extracts were injected onto a Thermo Electron LTQ-Orbitrap XL mass spectrometer equipped with an Eksigent nanoLC separation module. Samples were loaded onto a C_{18} trapping column at 10 µL/min using 0.2% formic acid (v/v) in water. Peptides were eluted onto a C_{18} analytical column (10 cm×150 µm i.d.) at 0.6 µl/min. Gradient elution was performed using a solvent system of 0.2% formic acid in water (A), and 0.2% formic acid in acetonitrile (B). Peptides were separated by gradient elution from 0 to 70% B in 60 minutes. For mass calibration, we used an internal lock mass [protonated $(Si(CH_3)_2O))_6$; m/z 445.12057]. In each data collection cycle, one full MS scan (m/z 300–2000) was acquired in the Orbitrap (60000 resolution setting, automatic gain control (AGC) target of 10^6), followed by 3 data-dependent MS/MS scans in the LTQ (AGC target 10000; threshold 5000) for the 3 most abundant ions and collision induced dissociation (CID) for fragmentation.

Chromatin immunoprecipitation (ChIP)

Extracts containing fragments for chromatin imunoprecipitation (ChIP) were prepared as follows. 200 ml of exponentially growing cells ($O.D._{600}$ of 0.6 to 0.8) in YPD were treated with 1% formaldehyde at room temperature for 10 minutes. Formaldehyde was quenched with 0.125 M of glycine and cells were washed three times in cold water. Pellets (approximately 1.2×10^9 cells) were resuspended in 1.2 ml of lysis buffer (50 mM HEPES-KOH pH 7.5, 140 mM NaCl, 1% Triton X-100, 0.1% Na-deoxycholate, 1 mM EDTA, 1 mM PMSF, 30 mM sodium butyrate, complete EDTA-free protease inhibitor cocktail, Roche), and split into three tubes. After adding one volume of glass beads to each sample, cells were disrupted using a bead beater (Disruptor Genie, Scientific Industries) at maximal speed for 2h at 4°C. After removing the glass beads, the lysates were transferred to fresh tubes and sonicated for 15 minutes (30 seconds ON, 30 seconds OFF) at high intensity in a Bioruptor (Diagenode) connected to a water cooler at 4°C. Lysates were clarified by centrifugation and pooled into a 2 ml tube. After addition of 800 µl of fresh lysis buffer and mixing, lysates were clarified again by centrifugation. 4 µl of lysate (1% of the whole cell extract, WCE) was kept aside as an input control. For immunoprecipitation, aliquots of 400 µl were prepared for each ChIP and mixed with the appropriate antibody: either 5 µl of anti-H3K4ac, 5 µl of anti-H3-C (Abcam ab1791), 3 µl of anti-H3K4me3 (Abcam ab8580) for at least 1h at 4°C. Before use, Dynabeads M-280 coupled to sheep anti-rabbit IgG (InVitrogen) (30 µl per ChIP) were washed in lysis buffer containing 5 mg/ml bovine serum albumin. The beads were added to each lysate and incubated at 4°C for at least 1 h. Beads were washed twice with lysis buffer, twice with lysis buffer containing 500 mM NaCl, twice in wash buffer (10 mM Tris-HCl pH 8.0, 250 mM LiCl, 0.5% Nonidet-P40, 0.5% Na-deoxycholate, 1 mM EDTA) and once in TE (10 mM Tris-HCl pH 8.0, 1 mM EDTA). To elute the DNA, 100 µl of a 10% Chelex 100 (Biorad) suspension in water was added to the beads (as well as to the 1% WCE) and incubated at 100°C for 10 minutes. Tubes were then cooled and treated with 0.2 µg/µl ribonuclease A at 50°C for 30 min, followed by 0.2 µg/µl proteinase K at 50°C for 30 min. Samples were incubated again at 100°C for 10 min to inactivate the proteinase K and then cooled down and spun down to get rid of debris. 80 µl of each supernatant was kept at −20°C for qPCR or ChIP-chip analysis.

ChIP-chip

All ChIP-on-chip datasets have been deposited in NCBI's Gene Expression Omnibus [106] and are accessible through GEO Series accession number GSE27307 (http://www.ncbi.nlm.nih.gov/geo/query/acc.cgi?acc = GSE27307). Samples were processed according to the Affymetrix protocol for amplification, fragmentation and labelling of DNA for hybridisation to a GeneChip *S. cerevisiae* Tiling 1.0R Array (www.affymetrix.com). All ChIP-chips were performed in triplicate from independent colonies. Pre-processing of the data was carried out with the Affymetrix Tiling Analysis Software with default settings at 200bp bandwidth and expressed as a $\log_2$ ratio of the ChIP signal obtained for modified H3 (K4ac or K4me3) over that obtained from non-modified C-terminal H3 ChIP. The datasets used in Figure 4C and Figure 5F, 5G were normalised using the standard score (Z-score) equation: $z=(x-\mu)/\sigma$, where x is the [$\log_2$ (H3K4(mod) / H3-C)] raw value for each probe; µ is the mean raw value of all probes and σ is the standard deviation of the raw values for all probes. The resulting datasets have a normal distribution with a mean value of 0 and a standard deviation value of 1, and thus can be compared directly on the same scales. Data was displayed on the UCSC genome browser with the October 2003 *S.cerevisiae* genome assembly (http://genome.ucsc.edu/). Systematic alignment of ChIP-chip data to gene promoters and terminators were performed using the database management tools provided in the web application Galaxy (http://main.g2.bx.psu.edu/) and graphics were created with R (http://www.r-project.org/).

Promoter enrichment analyses and Venn diagrams

Gene promoters were defined as a genomic region −500 bp to +100 bp relative to gene start. Promoters containing Z-score values above the threshold value (90^{th} percentile: $Z>1.28$; 80^{th} percentile: $Z>0.84$; 70^{th} percentile $Z>0.52$) were compared using the web application BioVenn (http://www.cmbi.ru.nl/cdd/biovenn/).

RNA extraction and expression analysis using microarrays

Total RNA was extracted from three independent colonies using the hot phenol method as described previously [107]. A total of 7 µg of RNA were processed for microarray analysis using the One-Cycle Target Labeling package from Affymetrix and hybridised to a GeneChip Yeast Genome 2.0 Array following the manufacturer's instructions (http://www.affymetrix.com/). Probe intensity data was pre-processed using the mas5 program of the R-Bioconductor software (http://www.bioconductor.org/index.html) [108]. The data from either *H3-K4R* or *set1*Δ mutants were normalised to their WT counterpart and the genes were sorted according to $\log_2$ fold change. The $\log_2$ fold change values for all genes are presented in Table S2 and represented graphically in Figure S6. For RT-qPCR analyses, 1 µg of total RNA was treated with DNase I, which was then inactivated following the manufacturer's instructions (DNA-free kit, Ambion). RT was performed using the First-Strand cDNA Synthesis Kit with M-MLV RT (Invitrogen) and oligo-dT primers, following the manufacturer's instructions.

Quantitative PCR

1 µl of the ChIP sample was mixed with 50 nM of region-specific primers and SYBR Green JumpStart Taq ReadyMix (Sigma) in a total volme of 20 µl and analysed on an Opticon real-time PCR machine (MJ Research/Bio-Rad). Relative binding values were extrapolated by subtracting the Ct of non-modified H3-C to that of modified H3 (K4ac or K4me3), and converting the ΔCt with the following formula: $x=2^{(-\Delta Ct)}$, where x represents the relative binding value of modified H3 on non-modified H3-C.

Supporting Information

Figure S1 Nicotinamide Treatment Increases H3K4ac in WT and *hst1*Δ cells. Whole-cell lysates from cells treated with 0, 5 or 25 mM nicotinamide for the indicated times were analysed by immunoblotting.
Found at: doi:10.1371/journal.pgen.1001354.s001 (0.40 MB TIF)

Figure S2 Genome-Wide Location of H3K4ac along the 16 *S. cerevisiae* Chromosomes. The $\log_2$ of the H3K4ac / H3 derived from ChIP-chip data was aligned to the chromosomes in the UCSC genome browser (http://genome.ucsc.edu). The graphs are drawn to scale for chromosome length, except for the chromosome XII, on which the repeated ribosomal DNA locus is represented only once on the array. The *y*-axis is scaled according to maximal and minimal values for each individual chromosome. In general, regions that are enriched (peaks) or depleted (troughs) for H3K4ac are interspersed and evenly distributed across all chromosomes. One notable exception is the ends of chromosome III, where large regions that extend from telomeres to beyond the silent mating type loci (*HML*α and *HMR*a; highlighted) are depleted in H3K4ac.
Found at: doi:10.1371/journal.pgen.1001354.s002 (2.00 MB TIF)

Figure S3 Localisation of H3K4ac, H3K4me3, -me2 and me1 at several genomic regions in yeast. The $\log_2$ of the H3K4ac / H3 derived from ChIP-chip data was aligned to the chromosomes in the UCSC genome browser and aligned with the H3K4me1, me2 and me3 data published previously [59]. Each vertical line represents one probe in the dataset and the intensity of the color is proportional to the enrichment of the modification. For clarity, only the probes with a $\log_2$ ratio above 0 are shown for each dataset.
Found at: doi:10.1371/journal.pgen.1001354.s003 (1.05 MB TIF)

Figure S4 Localisation of H3K4 Modifications (H3K4ac, H3K4me3, H3K4me2, H3K4me1) and RNA polymerase II (Pol II) in Human $CD4^+$ T Cells. ChIP-seq data from human $CD4^+$ lymphocytes previously published by the Zhao laboratory [19,51] were displayed on the UCSC genome browser (http://genome.ucsc.edu/). Genes are illustrated at the bottom of each panel with an arrow indicating the transcriptional start site and direction.
Found at: doi:10.1371/journal.pgen.1001354.s004 (2.50 MB TIF)

Figure S5 ChIP-qPCR confirmation of H3K4ac regulation by *SET1* at specific gene promoters. We performed ChIP against either H3K4ac (top row), H3K4me2 (middle row) or H3K4me3 (bottom row) in WT and *set1*Δ cells. We analysed the enrichment over three genomic regions by qPCR: *CPA2* (A), *ARG7* (B) and *FKH1* (C) which showed low, moderate and high increase in H3K4ac in *set1*Δ cells compared to WT in the coding region in our ChIP-chip analyses. Modification-specific ChIPs were normalised with ChIPs against non-modified H3-C using the same whole cell extract and experiments were done in biological triplicates.
Found at: doi:10.1371/journal.pgen.1001354.s005 (0.51 MB TIF)

Figure S6 Gene Expression Changes in *H3-K4R* and *set1*Δ Mutants Relative to WT Cells. All genes were color-coded and ranked according to $\log_2$ fold change in the *H3-K4R* strain or the *set1*Δ strain versus WT cells. On the right, the top and bottom part of the graph were cropped to reveal the general overlap between the genes that are up-regulated (yellow), but not down-regulated (blue). The right part of the figure contains the list of all genes with a fold-change equal or greater than two in the *H3-K4R* strain. A complete list of all the genes and their fold-change values is presented in Table S2.
Found at: doi:10.1371/journal.pgen.1001354.s006 (2.17 MB TIF)

Table S1 Yeast Strains Used in this Study.
Found at: doi:10.1371/journal.pgen.1001354.s007 (0.07 MB DOC)

Table S2 Genes and their fold-change values.
Found at: doi:10.1371/journal.pgen.1001354.s008 (1.59 MB XLS)

Acknowledgments

We are grateful to Drs. A. Morillon, S. Dent, M. Grunstein, J. Greenblatt, J. Boeke, and V. Géli for the gift of strains. We also thank L. Aragon, M. Leleu, P.-É. Jacques, S. Drouin, S. Lemieux, L. Game, J. Dennis, T. Bradley, P. Wijchers, R. Allshire, and members of the Festenstein and Verreault labs for helpful discussions.

Author Contributions

Conceived and designed the experiments: BG AV RJF. Performed the experiments: BG PD HHSL HA AI ÉB PT. Analyzed the data: BG PD PT. Contributed reagents/materials/analysis tools: BG HHSL KHH AI AV. Wrote the paper: BG AV RJF.

References

1. Kouzarides T (2007) Chromatin modifications and their function. Cell 128: 693–705.
2. Sun ZW, Allis CD (2002) Ubiquitination of histone H2B regulates H3 methylation and gene silencing in yeast. Nature 418: 104–108.
3. Dover J, Schneider J, Tawiah-Boateng MA, Wood A, Dean K, et al. (2002) Methylation of histone H3 by COMPASS requires ubiquitination of histone H2B by Rad6. J Biol Chem 277: 28368–28371.
4. Fischle W, Tseng BS, Dormann HL, Ueberheide BM, Garcia BA, et al. (2005) Regulation of HP1-chromatin binding by histone H3 methylation and phosphorylation. Nature 438: 1116–1122.
5. Jenuwein T, Allis CD (2001) Translating the histone code. Science 293: 1074–1080.
6. Turner BM (2002) Cellular memory and the histone code. Cell 111: 285–291.
7. Trelle MB, Jensen ON (2007) Functional proteomics in histone research and epigenetics. Expert Rev Proteomics 4: 491–503.
8. Brumbaugh J, Phanstiel D, Coon JJ (2008) Unraveling the histone's potential: a proteomics perspective. Epigenetics 3: 254–257.
9. Zhang L, Eugeni EE, Parthun MR, Freitas MA (2003) Identification of novel histone post-translational modifications by peptide mass fingerprinting. Chromosoma 112: 77–86.
10. Shilatifard A (2008) Molecular implementation and physiological roles for histone H3 lysine 4 (H3K4) methylation. Curr Opin Cell Biol 20: 341–348.
11. Ruthenburg AJ, Allis CD, Wysocka J (2007) Methylation of lysine 4 on histone H3: intricacy of writing and reading a single epigenetic mark. Mol Cell 25: 15–30.
12. Bernstein BE, Humphrey EL, Erlich RL, Schneider R, Bouman P, et al. (2002) Methylation of histone H3 Lys 4 in coding regions of active genes. Proc Natl Acad Sci U S A 99: 8695–8700.
13. Strahl BD, Ohba R, Cook RG, Allis CD (1999) Methylation of histone H3 at lysine 4 is highly conserved and correlates with transcriptionally active nuclei in Tetrahymena. Proc Natl Acad Sci U S A 96: 14967–14972.
14. Schneider R, Bannister AJ, Myers FA, Thorne AW, Crane-Robinson C, et al. (2003) Histone H3 lysine 4 methylation patterns in higher eukaryotic genes. Nat Cell Biol.
15. Schubeler D, MacAlpine DM, Scalzo D, Wirbelauer C, Kooperberg C, et al. (2004) The histone modification pattern of active genes revealed through genome-wide chromatin analysis of a higher eukaryote. Genes Dev 18: 1263–1271.
16. Santos-Rosa H, Schneider R, Bannister AJ, Sherriff J, Bernstein BE, et al. (2002) Active genes are tri-methylated at K4 of histone H3. Nature 419: 407–411.
17. Guenther MG, Levine SS, Boyer LA, Jaenisch R, Young RA (2007) A chromatin landmark and transcription initiation at most promoters in human cells. Cell 130: 77–88.
18. Ng HH, Robert F, Young RA, Struhl K (2003) Targeted recruitment of Set1 histone methylase by elongating Pol II provides a localized mark and memory of recent transcriptional activity. Mol Cell 11: 709–719.
19. Barski A, Cuddapah S, Cui K, Roh TY, Schones DE, et al. (2007) High-resolution profiling of histone methylations in the human genome. Cell 129: 823–837.

20. Pokholok DK, Harbison CT, Levine S, Cole M, Hannett NM, et al. (2005) Genome-wide Map of Nucleosome Acetylation and Methylation in Yeast. Cell 122: 517–527.
21. Liu CL, Kaplan T, Kim M, Buratowski S, Schreiber SL, et al. (2005) Single-Nucleosome Mapping of Histone Modifications in S. cerevisiae. PLoS Biol 3: e328. doi:10.1371/journal.pbio.0030328.
22. Zhang X, Bernatavichute YV, Cokus S, Pellegrini M, Jacobsen SE (2009) Genome-wide analysis of mono-, di- and trimethylation of histone H3 lysine 4 in Arabidopsis thaliana. Genome Biol 10: R62.
23. Flanagan JF, Mi LZ, Chruszcz M, Cymborowski M, Clines KL, et al. (2005) Double chromodomains cooperate to recognize the methylated histone H3 tail. Nature 438: 1181–1185.
24. Wysocka J, Swigut T, Xiao H, Milne TA, Kwon SY, et al. (2006) A PHD finger of NURF couples histone H3 lysine 4 trimethylation with chromatin remodelling. Nature 442: 86–90.
25. Li H, Ilin S, Wang W, Duncan EM, Wysocka J, et al. (2006) Molecular basis for site-specific read-out of histone H3K4me3 by the BPTF PHD finger of NURF. Nature 442: 91–95.
26. Shi X, Hong T, Walter KL, Ewalt M, Michishita E, et al. (2006) ING2 PHD domain links histone H3 lysine 4 methylation to active gene repression. Nature 442: 96–99.
27. Martin DG, Baetz K, Shi X, Walter KL, MacDonald VE, et al. (2006) The Yng1p plant homeodomain finger is a methyl-histone binding module that recognizes lysine 4-methylated histone H3. Mol Cell Biol 26: 7871–7879.
28. Shi X, Kachirskaia I, Walter KL, Kuo JH, Lake A, et al. (2007) Proteome-wide analysis in Saccharomyces cerevisiae identifies several PHD fingers as novel direct and selective binding modules of histone H3 methylated at either lysine 4 or lysine 36. J Biol Chem 282: 2450–2455.
29. Lan F, Collins RE, De Cegli R, Alpatov R, Horton JR, et al. (2007) Recognition of unmethylated histone H3 lysine 4 links BHC80 to LSD1-mediated gene repression. Nature 448: 718–722.
30. Matthews AG, Kuo AJ, Ramon-Maiques S, Han S, Champagne KS, et al. (2007) RAG2 PHD finger couples histone H3 lysine 4 trimethylation with V(D)J recombination. Nature 450: 1106–1110.
31. Vermeulen M, Mulder KW, Denissov S, Pijnappel WW, van Schaik FM, et al. (2007) Selective anchoring of TFIID to nucleosomes by trimethylation of histone H3 lysine 4. Cell 131: 58–69.
32. Sims RJ, 3rd, Millhouse S, Chen CF, Lewis BA, Erdjument-Bromage H, et al. (2007) Recognition of trimethylated histone H3 lysine 4 facilitates the recruitment of transcription postinitiation factors and pre-mRNA splicing. Mol Cell 28: 665–676.
33. Taverna SD, Ilin S, Rogers RS, Tanny JC, Lavender H, et al. (2006) Yng1 PHD finger binding to H3 trimethylated at K4 promotes NuA3 HAT activity at K14 of H3 and transcription at a subset of targeted ORFs. Mol Cell 24: 785–796.
34. Ooi SK, Qiu C, Bernstein E, Li K, Jia D, et al. (2007) DNMT3L connects unmethylated lysine 4 of histone H3 to de novo methylation of DNA. Nature 448: 714–717.
35. Huang Y, Fang J, Bedford MT, Zhang Y, Xu RM (2006) Recognition of histone H3 lysine-4 methylation by the double tudor domain of JMJD2A. Science 312: 748–751.
36. Pena PV, Davrazou F, Shi X, Walter KL, Verkhusha VV, et al. (2006) Molecular mechanism of histone H3K4me3 recognition by plant homeodomain of ING2. Nature 442: 100–103.
37. Santos-Rosa H, Schneider R, Bernstein BE, Karabetsou N, Morillon A, et al. (2003) Methylation of histone H3 K4 mediates association of the Isw1p ATPase with chromatin. Mol Cell 12: 1325–1332.
38. Roguev A, Schaft D, Shevchenko A, Pijnappel WW, Wilm M, et al. (2001) The Saccharomyces cerevisiae Set1 complex includes an Ash2 homologue and methylates histone 3 lysine 4. Embo J 20: 7137–7148.
39. Krogan NJ, Dover J, Khorrami S, Greenblatt JF, Schneider J, et al. (2002) COMPASS, a histone H3 (Lysine 4) methyltransferase required for telomeric silencing of gene expression. J Biol Chem 277: 10753–10755.
40. Miller T, Krogan NJ, Dover J, Erdjument-Bromage H, Tempst P, et al. (2001) COMPASS: a complex of proteins associated with a trithorax-related SET domain protein. Proc Natl Acad Sci U S A 98: 12902–12907.
41. Briggs SD, Bryk M, Strahl BD, Cheung WL, Davie JK, et al. (2001) Histone H3 lysine 4 methylation is mediated by Set1 and required for cell growth and rDNA silencing in Saccharomyces cerevisiae. Genes Dev 15: 3286–3295.
42. Nagy PL, Griesenbeck J, Kornberg RD, Cleary ML (2002) A trithorax-group complex purified from Saccharomyces cerevisiae is required for methylation of histone H3. Proc Natl Acad Sci U S A 99: 90–94.
43. Vitaliano-Prunier A, Menant A, Hobeika M, Geli V, Gwizdek C, et al. (2008) Ubiquitylation of the COMPASS component Swd2 links H2B ubiquitylation to H3K4 trimethylation. Nat Cell Biol 10: 1365–1371.
44. Dehe PM, Geli V (2006) The multiple faces of Set1. Biochem Cell Biol 84: 536–548.
45. Jiang L, Smith JN, Anderson SL, Ma P, Mizzen CA, et al. (2007) Global assessment of combinatorial post-translational modification of core histones in yeast using contemporary mass spectrometry. LYS4 trimethylation correlates with degree of acetylation on the same H3 tail. J Biol Chem 282: 27923–27934.
46. Zhang K, Siino JS, Jones PR, Yau PM, Bradbury EM (2004) A mass spectrometric "Western blot" to evaluate the correlations between histone methylation and histone acetylation. Proteomics 4: 3765–3775.
47. Nightingale KP, Gendreizig S, White DA, Bradbury C, Hollfelder F, et al. (2007) Cross-talk between histone modifications in response to histone deacetylase inhibitors: MLL4 links histone H3 acetylation and histone H3K4 methylation. J Biol Chem 282: 4408–4416.
48. Young NL, Dimaggio PA, Plazas-Mayorca MD, Baliban RC, Floudas CA, et al. (2009) High-throughput characterization of combinatorial histone codes. Mol Cell Proteomics.
49. Hazzalin CA, Mahadevan LC (2005) Dynamic acetylation of all lysine 4-methylated histone H3 in the mouse nucleus: analysis at c-fos and c-jun. PLoS Biol 3: e393. doi:10.1371/journal.pbio.0030393.
50. Kim T, Buratowski S (2009) Dimethylation of H3K4 by Set1 recruits the Set3 histone deacetylase complex to 5′ transcribed regions. Cell 137: 259–272.
51. Wang Z, Zang C, Rosenfeld JA, Schones DE, Barski A, et al. (2008) Combinatorial patterns of histone acetylations and methylations in the human genome. Nat Genet 40: 897–903.
52. Garcia BA, Hake SB, Diaz RL, Kauer M, Morris SA, et al. (2007) Organismal differences in post-translational modifications in histones H3 and H4. J Biol Chem 282: 7641–7655.
53. Suka N, Suka Y, Carmen AA, Wu J, Grunstein M (2001) Highly specific antibodies determine histone acetylation site usage in yeast heterochromatin and euchromatin. Mol Cell 8: 473–479.
54. Fillingham J, Recht J, Silva AC, Suter B, Emili A, et al. (2008) Chaperone control of the activity and specificity of the histone H3 acetyltransferase Rtt109. Mol Cell Biol 28: 4342–4353.
55. Rusche LN, Kirchmaier AL, Rine J (2003) The establishment, inheritance, and function of silenced chromatin in Saccharomyces cerevisiae. Annu Rev Biochem 72: 481–516.
56. Robert F, Pokholok DK, Hannett NM, Rinaldi NJ, Chandy M, et al. (2004) Global position and recruitment of HATs and HDACs in the yeast genome. Mol Cell 16: 199–209.
57. Hickman MA, Rusche LN (2007) Substitution as a mechanism for genetic robustness: the duplicated deacetylases Hst1p and Sir2p in Saccharomyces cerevisiae. PLoS Genet 3: e126. doi:10.1371/journal.pgen.0030126.
58. Karolchik D, Baertsch R, Diekhans M, Furey TS, Hinrichs A, et al. (2003) The UCSC Genome Browser Database. Nucleic Acids Res 31: 51–54.
59. Holstege FC, Jennings EG, Wyrick JJ, Lee TI, Hengartner CJ, et al. (1998) Dissecting the regulatory circuitry of a eukaryotic genome. Cell 95: 717–728.
60. Kirmizis A, Santos-Rosa H, Penkett CJ, Singer MA, Vermeulen M, et al. (2007) Arginine methylation at histone H3R2 controls deposition of H3K4 trimethylation. Nature 449: 928–932.
61. Dehe PM, Dichtl B, Schaft D, Roguev A, Pamblanco M, et al. (2006) Protein interactions within the Set1 complex and their roles in the regulation of histone 3 lysine 4 methylation. J Biol Chem 281: 35404–35412.
62. Schneider J, Wood A, Lee JS, Schuster R, Dueker J, et al. (2005) Molecular regulation of histone H3 trimethylation by COMPASS and the regulation of gene expression. Mol Cell 19: 849–856.
63. Morillon A, Karabetsou N, Nair A, Mellor J (2005) Dynamic lysine methylation on histone H3 defines the regulatory phase of gene transcription. Mol Cell 18: 723–734.
64. Dietvorst J, Brandt A (2008) Flocculation in Saccharomyces cerevisiae is repressed by the COMPASS methylation complex during high-gravity fermentation. Yeast 25: 891–901.
65. Carvin CD, Kladde MP (2004) Effectors of lysine 4 methylation of histone H3 in Saccharomyces cerevisiae are negative regulators of PHO5 and GAL1-10. J Biol Chem 279: 33057–33062.
66. Pinskaya M, Gourvennec S, Morillon A (2009) H3 lysine 4 di- and tri-methylation deposited by cryptic transcription attenuates promoter activation. Embo J 28: 1697–1707.
67. Xhemalce B, Kouzarides T (2010) A chromodomain switch mediated by histone H3 Lys 4 acetylation regulates heterochromatin assembly. Genes Dev 24: 647–652.
68. Baker SP, Grant PA (2007) The SAGA continues: expanding the cellular role of a transcriptional co-activator complex. Oncogene 26: 5329–5340.
69. Nagy Z, Tora L (2007) Distinct GCN5/PCAF-containing complexes function as co-activators and are involved in transcription factor and global histone acetylation. Oncogene 26: 5341–5357.
70. Vogelauer M, Wu J, Suka N, Grunstein M (2000) Global histone acetylation and deacetylation in yeast. Nature 408: 495–498.
71. Zhang W, Bone JR, Edmondson DG, Turner BM, Roth SY (1998) Essential and redundant functions of histone acetylation revealed by mutation of target lysines and loss of the Gcn5p acetyltransferase. Embo J 17: 3155–3167.
72. Collins SR, Miller KM, Maas NL, Roguev A, Fillingham J, et al. (2007) Functional dissection of protein complexes involved in yeast chromosome biology using a genetic interaction map. Nature 446: 806–810.
73. Han J, Zhou H, Horazdovsky B, Zhang K, Xu RM, et al. (2007) Rtt109 acetylates histone H3 lysine 56 and functions in DNA replication. Science 315: 653–655.
74. Driscoll R, Hudson A, Jackson SP (2007) Yeast Rtt109 promotes genome stability by acetylating histone H3 on lysine 56. Science 315: 649–652.
75. Schneider J, Bajwa P, Johnson FC, Bhaumik SR, Shilatifard A (2006) Rtt109 is required for proper H3K56 acetylation: a chromatin mark associated with the elongating RNA polymerase II. J Biol Chem 281: 37270–37274.

76. Li Q, Zhou H, Wurtele H, Davies B, Horazdovsky B, et al. (2008) Acetylation of histone H3 lysine 56 regulates replication-coupled nucleosome assembly. Cell 134: 244–255.
77. Chen CC, Carson JJ, Feser J, Tamburini B, Zabaronick S, et al. (2008) Acetylated lysine 56 on histone H3 drives chromatin assembly after repair and signals for the completion of repair. Cell 134: 231–243.
78. Masumoto H, Hawke D, Kobayashi R, Verreault A (2005) A role for cell-cycle-regulated histone H3 lysine 56 acetylation in the DNA damage response. Nature 436: 294–298.
79. Tang Y, Holbert MA, Delgoshaie N, Wurtele H, Guillemette B, et al. (2011) Structure of the Rtt109-AcCoA/Vps75 Complex and Implications for Chaperone-Mediated Histone Acetylation. Structure 19: 221–231.
80. Burgess RJ, Zhou H, Han J, Zhang Z (2010) A role for Gcn5 in replication-coupled nucleosome assembly. Mol Cell 37: 469–480.
81. Didion T, Regenberg B, Jorgensen MU, Kielland-Brandt MC, Andersen HA (1998) The permease homologue Ssy1p controls the expression of amino acid and peptide transporter genes in Saccharomyces cerevisiae. Mol Microbiol 27: 643–650.
82. Nielsen PS, van den Hazel B, Didion T, de Boer M, Jorgensen M, et al. (2001) Transcriptional regulation of the Saccharomyces cerevisiae amino acid permease gene BAP2. Mol Gen Genet 264: 613–622.
83. Schmidt A, Hall MN, Koller A (1994) Two FK506 resistance-conferring genes in Saccharomyces cerevisiae, TAT1 and TAT2, encode amino acid permeases mediating tyrosine and tryptophan uptake. Mol Cell Biol 14: 6597–6606.
84. Zhu X, Garrett J, Schreve J, Michaeli T (1996) GNP1, the high-affinity glutamine permease of S. cerevisiae. Curr Genet 30: 107–114.
85. Rusche LN, Rine J (2001) Conversion of a gene-specific repressor to a regional silencer. Genes Dev 15: 955–967.
86. McCord R, Pierce M, Xie J, Wonkatal S, Mickel C, et al. (2003) Rfm1, a novel tethering factor required to recruit the Hst1 histone deacetylase for repression of middle sporulation genes. Mol Cell Biol 23: 2009–2016.
87. Pijnappel WW, Schaft D, Roguev A, Shevchenko A, Tekotte H, et al. (2001) The S. cerevisiae SET3 complex includes two histone deacetylases, Hos2 and Hst1, and is a meiotic-specific repressor of the sporulation gene program. Genes Dev 15: 2991–3004.
88. Xie J, Pierce M, Gailus-Durner V, Wagner M, Winter E, et al. (1999) Sum1 and Hst1 repress middle sporulation-specific gene expression during mitosis in Saccharomyces cerevisiae. Embo J 18: 6448–6454.
89. Brachmann CB, Sherman JM, Devine SE, Cameron EE, Pillus L, et al. (1995) The SIR2 gene family, conserved from bacteria to humans, functions in silencing, cell cycle progression, and chromosome stability. Genes Dev 9: 2888–2902.
90. Derbyshire MK, Weinstock KG, Strathern JN (1996) HST1, a new member of the SIR2 family of genes. Yeast 12: 631–640.
91. Venkatasubrahmanyam S, Hwang WW, Meneghini MD, Tong AH, Madhani HD (2007) Genome-wide, as opposed to local, antisilencing is mediated redundantly by the euchromatic factors Set1 and H2A.Z. Proc Natl Acad Sci U S A 104: 16609–16614.
92. Crampton A, Chang F, Pappas DL, Jr., Frisch RL, Weinreich M (2008) An ARS element inhibits DNA replication through a SIR2-dependent mechanism. Mol Cell 30: 156–166.
93. Mead J, McCord R, Youngster L, Sharma M, Gartenberg MR, et al. (2007) Swapping the gene-specific and regional silencing specificities of the Hst1 and Sir2 histone deacetylases. Mol Cell Biol 27: 2466–2475.
94. Frye RA (2000) Phylogenetic classification of prokaryotic and eukaryotic Sir2-like proteins. Biochem Biophys Res Commun 273: 793–798.
95. Agalioti T, Chen G, Thanos D (2002) Deciphering the transcriptional histone acetylation code for a human gene. Cell 111: 381–392.
96. Lachner M, O'Carroll D, Rea S, Mechtler K, Jenuwein T (2001) Methylation of histone H3 lysine 9 creates a binding site for HP1 proteins. Nature 410: 116–120.
97. Bannister AJ, Zegerman P, Partridge JF, Miska EA, Thomas JO, et al. (2001) Selective recognition of methylated lysine 9 on histone H3 by the HP1 chromo domain. Nature 410: 120–124.
98. Shankaranarayana GD, Motamedi MR, Moazed D, Grewal SI (2003) Sir2 regulates histone H3 lysine 9 methylation and heterochromatin assembly in fission yeast. Curr Biol 13: 1240–1246.
99. Nakayama J, Rice JC, Strahl BD, Allis CD, Grewal SI (2001) Role of histone H3 lysine 9 methylation in epigenetic control of heterochromatin assembly. Science 292: 110–113.
100. Rea S, Eisenhaber F, O'Carroll D, Strahl BD, Sun ZW, et al. (2000) Regulation of chromatin structure by site-specific histone H3 methyltransferases. Nature 406: 593–599.
101. Morris SA, Rao B, Garcia BA, Hake SB, Diaz RL, et al. (2007) Identification of histone H3 lysine 36 acetylation as a highly conserved histone modification. J Biol Chem 282: 7632–7640.
102. Pinskaya M, Morillon A (2009) Histone H3 lysine 4 di-methylation: A novel mark for transcriptional fidelity? Epigenetics 4.
103. Kushnirov VV (2000) Rapid and reliable protein extraction from yeast. Yeast 16: 857–860.
104. Edmondson DG, Smith MM, Roth SY (1996) Repression domain of the yeast global repressor Tup1 interacts directly with histones H3 and H4. Genes Dev 10: 1247–1259.
105. Drogaris P, Wurtele H, Masumoto H, Verreault A, Thibault P (2008) Comprehensive profiling of histone modifications using a label-free approach and its applications in determining structure-function relationships. Anal Chem 80: 6698–6707.
106. Edgar R, Domrachev M, Lash AE (2002) Gene Expression Omnibus: NCBI gene expression and hybridization array data repository. Nucleic Acids Res 30: 207–210.
107. Schmitt ME, Brown TA, Trumpower BL (1990) A rapid and simple method for preparation of RNA from Saccharomyces cerevisiae. Nucleic Acids Res 18: 3091–3092.
108. Gentleman RC, Carey VJ, Bates DM, Bolstad B, Dettling M, et al. (2004) Bioconductor: open software development for computational biology and bioinformatics. Genome Biol 5: R80.